Using stable oxygen isotope stratigraphy to construct an age model for the Pliocene section of the 'Hank' North Sea sediment core

MSc thesis Damian Smits

Supervisors:
Francien Peterse, Emily Dearing Crampton-Flood, Lars Noorbergen and Lucas Lourens

Utrecht University

May 2018

Abstract

The Pliocene period is a good analogue for future climate. Firstly, CO_2 concentration in the atmosphere was similar to modern day values. Furthermore, temperatures were slightly higher (ΔT = 2-3 °C), something which is expected to happen in the future due to an enhanced greenhouse effect. The North Atlantic Ocean is crucial in controlling global climate, because North Atlantic ocean circulation has a major impact on Northern hemisphere glaciation. During the Pliocene, large parts of the Netherlands were submerged in a shallow sea. Previous studies of the southern North Sea Basin (Hank core) that have reconstructed sea surface temperature reconstructions, among other proxies, have yielded mixed results. An independently calibrated age model will aid in understanding trends in terrestrial and marine proxies, and will crucially provide a framework for the timing of trends observed in the proxy records. To this aim, oxygen and carbon isotope ratios of foraminifera in the Hank succession were analyzed. The species *Cassidulina Laevigata* and *Bulimina Aculeata*, both endobenthic, were studied. The resulting age model presented in this study is subject to a number of uncertainties, mostly caused by the core's proximal location to the coast. Nevertheless, with support of other terrestrial and marine proxies, as well as a seismic section, a representative age model could be created that agrees with previous proxies and age estimations.

Table of Contents Page

1. Introduction

1.1 Pliocene climate

The Pliocene (5.3-2.6 Ma) is a good analogue for future climate for several reasons. Firstly, the atmospheric concentration of carbon dioxide (CO_2), a notorious greenhouse gas, was comparable to present CO_2 concentrations (approximately 380 ppm; Dowsett et al., 2009, Raymo et al., 1996). Following that, the distribution of the continents during the Pliocene was similar to modern day (Schepper et al., 2014). However, global temperature was higher during the Pliocene than it is now (ΔT = 2-3 °C; Robinson et al., 2008), prompting the necessity of generated detailed Pliocene climate reconstructions, in order to better inform future climate projections.

During the late Pliocene, transitioning into the Pleistocene, climate cooled gradually, due to uplift of the Tibetan plateau (Rea et al., 1998). One of the most striking features of the Plio-Pleistocene transition is the gradual cooling that spun from the late Neogene to the Holocene (Mudelsee & Raymo, 2005). Moreover, at the end of the Pliocene, glacial-interglacial cycles begin to exhibit different features than before. One of these features is the increased expression of orbital forcing, as seen from higher amplitude obliquity cycles in the global $\delta^{18}O$ stack (Lisiecki & Raymo, 2007, Fig. 1).

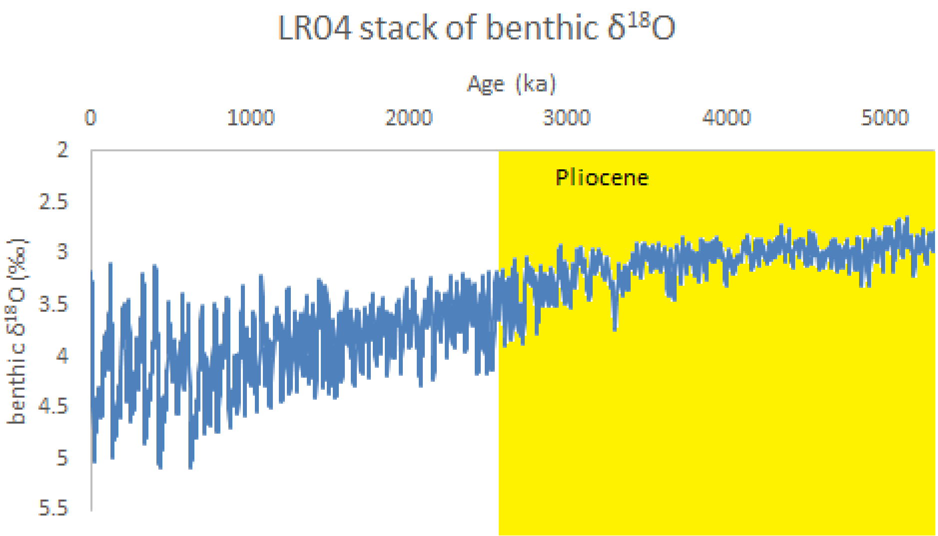

Figure 1. Benthic $\delta^{18}O$ stack, composed of 57 globally distributed benthic $\delta^{18}O$ records (Lisiecki and Raymo, 2005).

A relatively complete archive of Pliocene glacial-interglacial climate is derived from marine sediment cores and is predominantly made up of sea surface temperature (SST) reconstructions (Dowsett, 2007; Dowsett et al., 1996). Conversely, there is relatively little information of Pliocene terrestrial climate, due in part to the increased prevalence of hiatuses on land, as well as a relative lack of continental temperature proxies (Schepper et al., 2014).

1.2 Hank Succession

For this thesis, sediment samples recovered from a borehole near the village of Hank (Northwestern North-Brabant) will be analyzed. These samples range from the Early Pliocene (>4.5 Ma) to the Early Pleistocene (>2.5 Ma). During this time, the eustatic sea level was higher (Raymo et al., 2011), due to the lack of an ice shelf on Greenland (Lisiecki and Raymo, 2005). Local (relative) sea level may have been higher due to subsidence of the coast and proto-Rhine delta dynamics. The sediments from this borehole were therefore deposited proximal to the coast. The Hank site lies within the Roer valley Graben meaning that it lies lower than its surroundings. This makes this location a likely sediment deposit basin (Van Balen et al., 2000).

The Hank succession is thus part of the past North Sea. This site was selected due to its location close to the mouth of the proto-Rhine river. It receives high amounts of terrestrial organic matter, including biomarkers, such as branched glycerol dialkyl glycerol tetraether lipids (brGDGTs) that allow reconstructing terrestrial paleo temperatures (e.g. Weijers et al 2007 GCA and Science). Likewise, the sediments also contain high amounts of marine organic carbon, including marine biomarkers that can reconstruct SST, enabling for direct land-sea comparisons.

The importance of understanding the link between marine and terrestrial climate is underpinned by the idea that the North Atlantic Ocean is crucial in controlling global climate. Ocean circulation has a major impact on northern hemisphere glaciation (Dowsett et al., 2009, De Schepper et al., 2014). This operates as a feedback mechanism, as global climate itself influences ocean circulation. During the Pliocene warm period (~3.3-3.0 Ma, Raymo et al., 2006), ocean circulation was stronger (Ravelo & Andreasen, 2000), something which can be expected for the future as the enhanced greenhouse effect continues to warm the climate.

Previous work in the Pliocene North Sea has produced a record of past temperature variation in Northwestern Europe, using branched GDGTs (Dearing Crampton-Flood et al., 2018). The authors' main interest was to reconstruct paleo terrestrial temperature records. The terrestrial temperature record corresponds with expectations regarding trends in past temperature, and matches well with palynological data including dinocyst and pollen assemblages (Munsterman, 2016). However, the organic proxies for SSTs (TEX_{86} and $U_{37}^{k'}$), analyzed in the same sediment core to enable a land-sea temperature comparison, follow different trends than the terrestrial temperature record (Fig. 2).

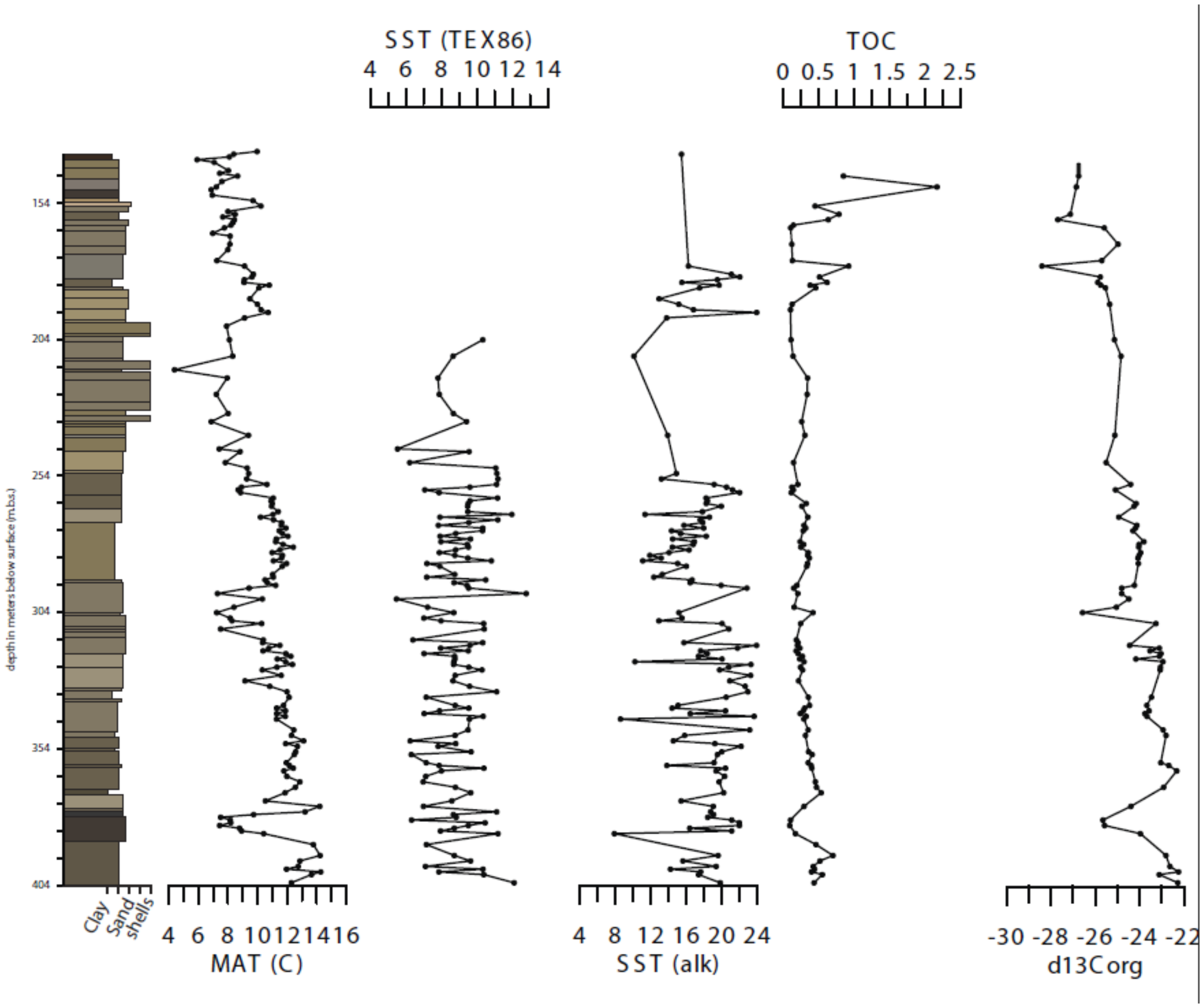

Figure 2. Proxies from previous studies on the Hank Core, North Sea; a) mean annual temperature (MAT), b) Sea Surface Temperature (TEX_{86}) and c) $U_{37}^{k'}$). d) Total Organic Carbon (TOC) and e) $\delta^{13}C$ of bulk organic material.(data: Dearing Crampton-Flood et al., 2018)

The interpretation of the terrestrial and marine temperature records (and palynology records) will be facilitated by the creation of an independent age model, to provide a framework for the timing of trends observed in the proxy records. The current age model (Dearing Crampton Flood et al., 2018; Figure 3) for Hank is based on first and last dates of occurrence of dinoflagellate species (Meijer et al., 2006, Louwye et al., 2004, De Schepper et al., 2015, Versteegh, 1997, Kuhlmann et al., 2006, Londeix et al., 2015, Mudie, 1987).

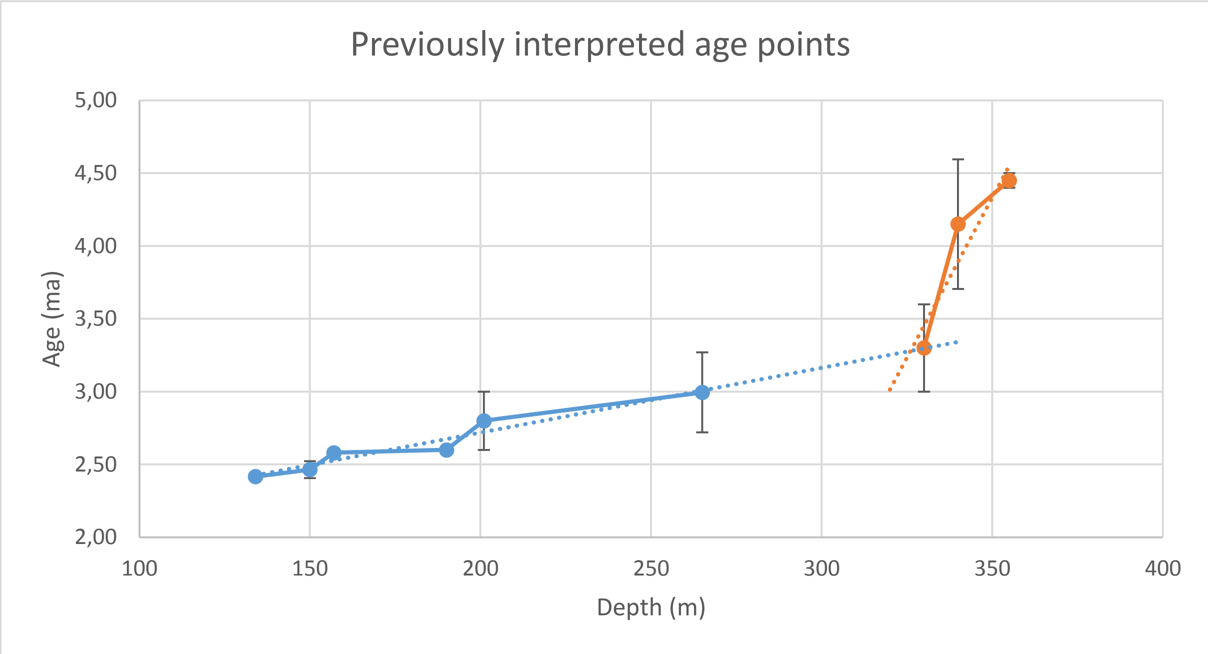

*Figure 2. Age points determined prior to this study (*Dearing Crampton Flood et al., 2018*). Extrapolated trendlines are used to convert depth to age for frequency analysis. No trend line is shown between 265 and 330 m due to a (sudden) change in sedimentation rate. Their intersection point indicates a possible hiatus.*

The data points in Fig. 2 may only be interpreted as an estimate. The current age model needs to be improved, as there is a large uncertainty range for almost all individual age points. Furthermore, the resolution is quite low, especially for the interval above 330 m, where sedimentation rate increases rapidly. This may be indicative of a hiatus, but the current age model does not permit a precise interpretation of where exactly this hiatus is found. Nevertheless, this initial age-depth model demonstrates that there is a strong change in sedimentation rate in this record from the North Sea. Therefore, two linear trends are established, one for the faster sedimentation rate (~40.7 kyr /m), and one for the slower (~2.2 kyr / m). As a result, the bottom of the core (where sedimentation rates are lowest), has a much lower resolution compared to the upper formations. Because the sedimentation rate supposedly changes rather suddenly between 275 and 330 meters, no linear trend is proposed for that interval.

It must be stipulated that the age points presented in Fig. 2 have a large uncertainty range, between 10kyr and half a million years. This age model is largely based on palynology, which is not sufficient for the purpose of creating an age model. Small scale local climatic effects may significantly alter the record. Creating an age model solely based on these points is therefore not ideal. Consequently, frequency analysis interpretation may be more difficult, due to the imprecise ages in the current model, that will be reflected in the resulting frequency analysis.

The terrestrial temperature record and SST records may thus benefit from comparison with established proxy records to constrain the timing of the events and trends observed in the proxy records. Stable isotope ratios of foraminifera have been proved to be useful tools for analyzing and reconstructing paleoclimate (Shackleton et al., 1984, Raymo et al., 2006).

Stable oxygen isotopes are a useful tool in this regard as they reflect surrounding water temperatures, as well as salinity and global ice volume effects. When ice forms, it prefers to take up ^{16}O over ^{18}O, due to ^{16}O being the lighter isotope of the two. Also, the amount of ^{18}O decreases by one per mille as temperature increases by 4.2°C (Ruddiman, 2014). Changes in salinity correlate positively with ^{18}O abundance, as an increase in salinity generally coincides with an increase in ^{18}O.

As foraminifers get preserved in the sediment, oxygen isotope ratios ($\delta^{18}O$) describing climate during their lifespan also get preserved. A global composite stack composed of over 50 open marine records has been compiled by Lisiecki and Raymo (2005; LR04), and spans the last 5.3 million years. By comparing the Late Pliocene $\delta^{18}O$ signatures of this study with the LR04 stack, an age model for specific sediment intervals may be established.

A $\delta^{13}C$ record resulting from analysis on forams can serve as a way to verify phenomena observed in the $\delta^{18}O$ record, especially in this Southern North Sea Basin (SNSB) case. In the majority of open marine sediment sequences, $\delta^{13}C$ shows the opposite trend to $\delta^{18}O$ (Noorbergen, 2015). In response to glacial and interglacial climate forcing, lighter $\delta^{13}C$ should correlate with heavier $\delta^{18}O$. Therefore, for a location where the isotopic composition of foraminifera is altered solely by glacial-interglacial cyclicity, the $\delta^{18}O$ and $\delta^{13}C$ of foraminifer tests records show a negative correlation. This is caused by the relative enrichment in ^{12}C of OC reaching the oceans during glacials, effectively lowering the $\delta^{13}C$ of OC stored in marine sediments (Ruddiman, 2014). During photosynthesis, plants and trees prefer the lighter ^{12}C over the heavier ^{13}C. A $\delta^{18}O$ record for hank has not yet been created, due to its location proximal to the coast. Freshwater input from the proto-rhine river delta tends to alter isotopic composition of a foraminifer's test (Noorbergen, 2013).

The main objective of this research is to create an age model based on stable oxygen isotope stratigraphy. The Foraminifer species *Cassidulina laevigata, Bulimina aculeata* are selected, because they burrow deeper in the sediment, and are thus less expected to be altered by fresh water input. Stable carbon isotopes will also be considered. By comparing our isotope record with the global $\delta^{18}O$ benthic stack (Lisiecki and Raymo, 2005, Fig. 1), presence of Late Pliocene glacial-interglacial climate cycles in a coastal sediment succession of the North Sea Basin will be tested.

2. Materials and methods

2.1. Sample collection and succession description

Sediments were retrieved in 2001, using an air lift drilling method. During the procedure, air was injected into the drill string, which created an air pressure gradient in the core. Material was then collected from the inherent upward flow. This way, a sample was taken every meter. However, because of the drilling method , there was an uncertainty of one meter every meter.

The part of the sediment succession used for isotope analysis in this study was composed of two main formations: The Breda formation (404-388 m) and the Oosterhout formation (388-157 m). Data from previous studies were more extensive and also described a large part of the Formation of Maassluis (Mensink and Mensovic, 2003).

Grain sizes varied between clay and very fine sand. There were several layers spanning multiple samples that consisted almost completely of larger shell fragments (so-called crags). The Breda Formation at the lower part of the core was characterized by a dark colored loamy layer (Fig. 4). The lower part of the Oosterhout formation still consisted of dark, more greenish sediment, but had more

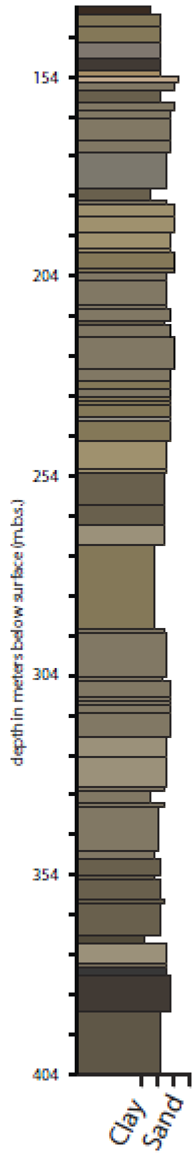

Figure 4. Hank lithology showing real colors.

coarse material. This greenish color was caused by an enhanced amount of glauconite, a greenish mica found commonly in north sea sediments (Munsterman & Brinkhuis, 2004). High amounts of glauconite can render sediments radioactive, due to enhanced presence of the radioactive ^{40}K isotope.

Upwards in the Oosterhout formation, the sediment became progressively lighter-colored. The first crags occured at 234 meters, after which they became more common. The borehole description has pinpointed 240 meters to 197 meters as a subgroup called the "Laagpakket van Sprundel". This crag is characteristic for the Southwest of the Netherlands (Ebbing & De Lang, 2003). At 157 meters was the base of the Maassluis Formation, which was characterized by darker (brownish) and more sandy material than the underlying Oosterhout Formation.

Each sample represented a one m interval of the core, for a total of 268 m. Of each sample, around 80 g of sediment was taken. Further treatment of these samples is mostly based on same methods used for samples of a comparable study in the Southern North Sea area (Noorbergen, 2013).

2.2 Seismic section

The visible part of the Breda Formation in the seismic section showed that the depositional environment was open marine (Figure 5). During deposition of the Oosterhout formation, the environment shifted gradually from open marine to more shallow. The bottom of the Oosterhout formation is characterized by relatively slow sedimentation rates compared to the top, which is indicative of this open marine environment. Below 295 meters lies a sequence of tightly packed formations, from 340 meters upwards. An unconformity lies at around 320 meters. This was stipulated by sudden increases in GR, SP and resistivity (Fig. 12, see results section 3.5).

The sediment coarsened upwards from 295 to 210 m, indicative of a prograding delta front. This is confirmed by the seismic section (Fig. 5). Between approximately 290 and 230m, the delta had migrated to the West so that sediments were now deposited as oblique clinoforms. Above 210 meters, thin layers sediments are deposited on top of each other in a shallow marine environment, on the topset part of the delta. Just below the border between the Oosterhout and Maassluis formation, disturbed sediment layers are likely reflecting channel incisions.

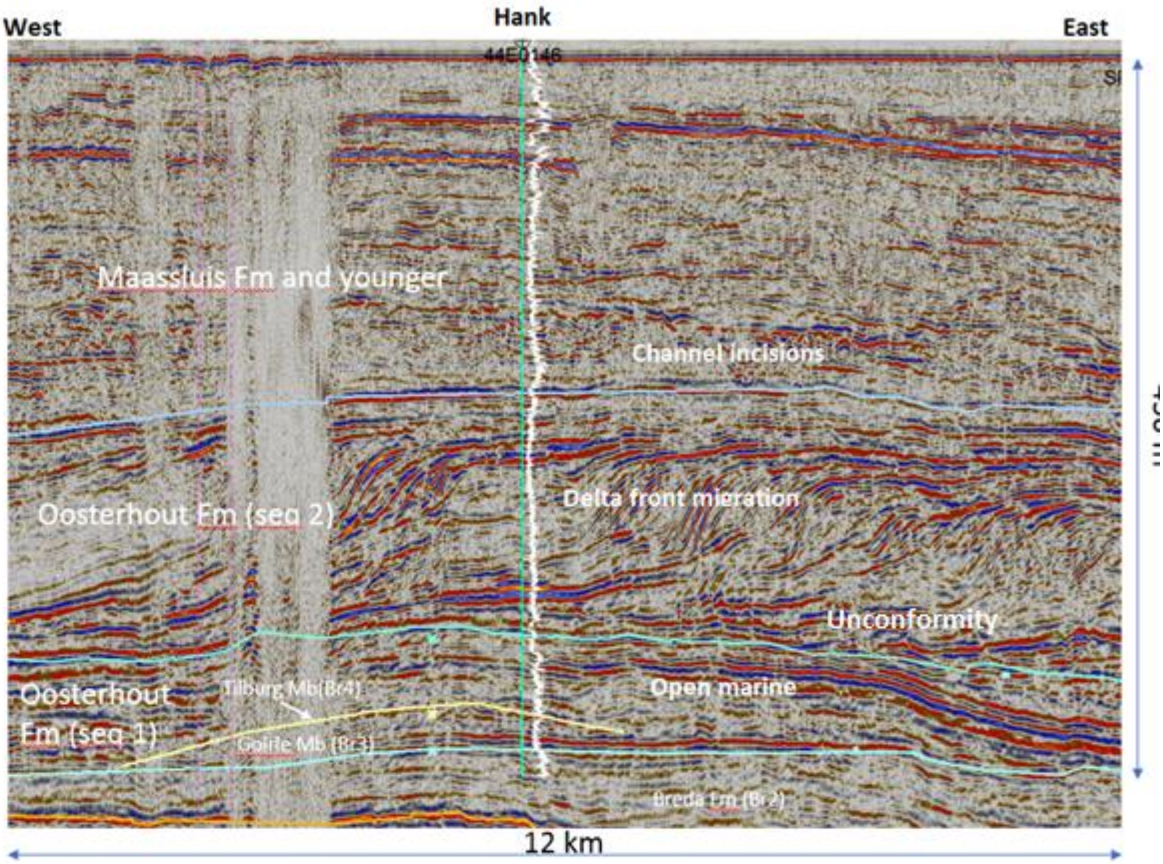

Figure 5. Seismic section near Hank, white graph indicates gamma ray log (seismic section retrieved from Dirk Munsterman, personal communication).~~.~~

2.3 Laboratory work

Around 40 – 60 grams of subsamples were submerged in water for several minutes to loosen the clumped material. Afterwards, sieving was used to divide the subsamples into three different fractions. Fractions 125 and 63 µm were chosen because the foraminifers used for analysis generally were the same size as fine to very fine sand.

2.3.1 Foram Picking and washing

Around one fourth of a teaspoon of sediment of the largest fraction (larger than 125 µm) was spread across a black plate (~45cm^2) for picking under a microscope. Foraminifers of the endobenthic species *Cassidulina laevigata*, *Bulimina aculeata* (Fig. 6), *Cibicides lobatulus* and *Elphidiella hannai* were picked. One drawback of using endobenthic species was that they might not give a clear representation of the overlying water column, as they are buried deep within the sediment (Fontanier et al., 2001, McCorkle et al., 1990). Conversely, endobenthic species may reflect the average isotope signal of pore waters around which they burrow (Mackensen et al., 2000). As a result of the proximal coast location of Hank, surrounding waters may have been turbulent and the sediment deposited prone to reworking, damaging and misplacing foraminifers. Since the depositional environment was located near a river delta, and therefore proximal to the coast, these species were selected.

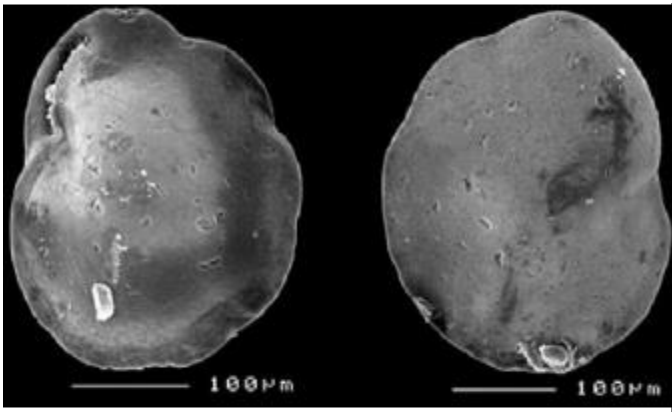

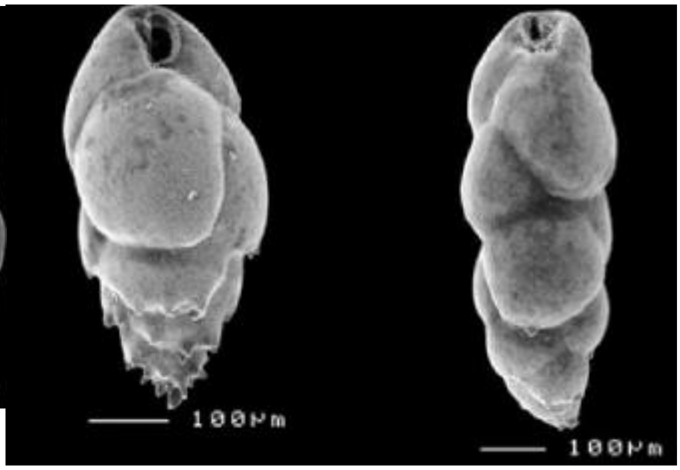

Figure 6. Picture of Cassisulina Laevigata (Left), and Bulimina eculeata (bottom) taken from Noorbergen, 2013.

The succession spanned the early Pleistocene to the Early Pliocene. This means that the complete record can be classified as biostratigraphic zones FA and FB (Doppert, 1980). These zones were not only defined by their age, but they also provided an overview of species abundance through time. No results are generated for stable isotopes on samples above 204 meters, because *Cassudilina laevigata* or *Bulimina aculeata* could not be found. Only a few samples from 136 to 200 meters were sieved and analyzed, because it was concluded that these samples fell in the Pleistocene section, and therefore may not contain any relevant forams for analysis.

For $\delta^{18}O$ analysis, at least five to eight specimens of each species were picked. Individual species of *Cassidulina* weighed around two to four micrograms each. For analysis, a total weight of at least 10 micrograms was required. Other species, such as *Bulimina,* were heavier, at more than ten micrograms per individual. It was decided that multiple individual specimens of *Bulimina* were needed, as a single specimen may have an altered isotope composition due to, for instance, reworking of the sediment. Not every individual foraminifer was selected or considered useful for analysis. Most of these specimens were either heavily damaged, reworked (seen by dark grayish color, instead of the usual white), or had calcite or metal oxide crystals on their surface. Species that were picked were generally the same size, as they likely reflect the same lifespan, and thus a similar period for the water record (Noorbergen, 2013). Forams with the same lifespan should have similar isotopic composition, as they describe the water column over supposedly the same time. Juvenile (small-sized) forams were generally avoided. They were recognizable by their smaller size and an irregular and incomplete pattern of chambers and “triangles” (Fig. 6).

Washing foraminifers was achieved by putting individual specimens on a glass plate, and grouping them together in 2 ml plastic vials. Using a pipette, 250 µl water was added. This was done slowly, as to not suspend the specimens in the water. Vials were put in an ultrasonic vibration bath for 5 seconds to remove any carbonates stuck to the surface of the foram. The excess carbonate material was removed with a pipette. This procedure was repeated twice. Afterwards, the samples were stored in the oven at 40°C, for at least 24 hours.

2.3.2 Crushing, weighing and flushing

Initially, samples were crushed before washing. This treatment would have resulted in a more reliable isotope record, because material stuck inside the chambers of the forams themselves would also have been removed. However, crushing forams resulted in a large loss of available material. As there was not enough material left for analysis for most samples that were crushed, it was decided that no further samples were crushed. All the data presented in this thesis is from non-crushed forams.

Forams were weighed using a Mettler Toledo balance with an accuracy of 1µg. Samples were generally between 10 and 60 µg, with a few exceptions. Standards, including Vienna Pee Dee belemnite (VPDB), were also weighed. Standards with a known isotopic ratio ($\delta^{18}O$ = -2.2‰, $\delta^{13}C$ = 1.95‰) were used to correct the sample $\delta^{18}O$ values. This was done by adding these standard values to the average sample measurement values.

Forams and standards were put into individual vials, closed with an airtight lid. These vials were flushed with helium for at least 5 minutes, by inserting a needle through a rubber in the middle of the lid. There was an air flow rate of at least 20ml/minute.

2.3.3 Isotope-ratio mass spectrometry

Vials were then placed in a Thermo gas bench II, as soon as possible after flushing with He. This gas bench punctured the top of the vial with a thin needle and inserted a small quantity of phosphoric acid to dissolve the forams. CO_2 released by this process was then led to a Delta V mass spectrometer via a thin tube. This gas is then ionized (CO^{2+}). Small quantities of this gas were then inserted in the mass spectrometer via a loop. This ensured being able to carry out more measurements per sample.

The ionized gas was accelerated and shot through several lenses, creating a thin beam. By a magnetic field, this beam was separated into different masses. An array of faraday cups then collected these masses, detecting them.

Two types of output were generated by carrying out mass spectrometry: stable oxygen isotopes and stable carbon isotopes. Three molecular masses were measured: 44, 45 and 46 m/z.

2.4 Data analysis

Oxygen isotope ratios for each sample were calculated by the following equation:

$$\delta^{18}O = \frac{\delta^{18}Os - \delta^{18}O_{\ standard}}{\delta^{18}O_{\ standard}} * 1000‰$$

Where:

- $\delta^{18}O$ resembled the eventual data (in ‰) used for comparison with Lisiecki and Raymo's data (2005).
- $\delta^{18}O_s$ was the isotope values of the samples, measured by the mass spectrometer.
- $\delta^{18}O_{standard}$ were the isotope values measured on the standards.

Data was plotted using a 7-point moving average, along with a record where one standard deviation was added and one where it was subtracted from the moving average. Any data points lying outside of the range between these two plots were removed and not taken into account later this study. Both the carbon and the oxygen isotope data was removed, as they result from the same sample and measurement.

2.5 Frequency analysis

Tuning could be done after carrying out a frequency analysis on the data, which was now in the time domain. Frequency analysis is only carried out on the part from around 300 to 200 meters, because resolution in the bottom part of the core is too low to capture smaller Milankovic scale climate (~23 and ~41 kyr) variability. Analyseries, software especially made for this purpose, was used for this (Paillard et al., 1996). By inputting the data, detrending it and running a Blackman-Tukey analysis, a frequency against power spectrum is generated. Afterwards, the data was resampled, making it usable for filtering. The data was Gaussian filtered around the most dominant peaks. These filters could also be compared by filters from the LR04 stack, whose data was filtered around the same peaks (Lisiecki and Raymo, 2005).

2.6 Other Proxies

The gamma ray log was a clue to unravelling whether the environment was more marine or more terrestrial. Gamma ray reflects the amount of clay minerals within the sediment (Rider, 1986). This could also be seen for the most part when looking at the lithological core description. It may not always coincide exactly, because glauconite abundance may slightly alter the Gamma ray values. For example, between 313 and 311 meters, there was a layer with a high amount of glauconite, while the layers above and below have low amounts of glauconite. A low value corresponds generally to more sandy sediments. Sandy sediments are expected to form at low stands, as the river can prograde further within the marine basin. There is a gradual rise in Gamma ray starting from around 240m, going deeper into the core. This also demonstrates that the environment was more marine in the deeper interval of the core.

Furthermore, previous data on the Hank core was used to pinpoint any possible events that happened during the Pliocene and Pleistocene, such as glacials. This data consists of mean annual temperature (MAT), previous results on SST ($U_{37}^{k'}$), $\delta^{13}C$ of organic material, Branched and Isoprenoid tetraether (BIT) index, the Gamma Ray values (GR), Spontaneous Potential (SP) and Resistivity (RES). Results for SST (TEX_{86}) are not considered in this study as those results were concluded to be not reliable (Boschman, 2016). Resistivity reflects the sediment's ability to resist an electric current. Formation waters that have relatively high salinity have a higher conductivity. To use the resistivity, the whole resistivity record had to be detrended, because formation water salinity naturally increases with depth. After detrending, the resistivity roughly indicates lithology and porosity of the sediment. A higher resistivity generally reflects lower porosity. Resistivity also rises when shale becomes more dominant in subsurface sediments. When pore water is present, the surface of clay minerals get negatively charged, to which the water physically binds. In contrast, a lower resistivity indicates a sandy sediment layer (Rider, 1986).

Finally, the ratio between sporomorphs and dinoflagellates was a useful tool in determining shifts from terrestrial to marine environments, and vice versa. A high abundance of sporomorphs relative to dinoflagellates indicates a more terrestrial depositional environment.

Principal Component Analysis (PCA) was carried out on all previously mentioned proxies, using the C2 software (Juggins, 2007). This was needed to be able to give a detailed and clear overview of correlations between proxies. For this analysis, only samples which had data ready for each proxy was accepted. This means that, in total, 54 samples were analyzed. For the interval between 200-382 m, proxies such as MAT, had relatively few data points compared to our isotope data. This resulted in a lower overall sample size for PCA analysis. Data from organic $\delta^{13}C$ was omitted completely, as there were too few data points to get a reliable PCA.

Lastly, features or phenomena that were striking when looking through a microscope may have to be considered. These could, for instance, consist of changes in lithology or species abundance. These can be found in appendix A.

The construction of the age model is based on multiple factors. There are several age points already determined in a previous study (Dearing Crampton Flood et al., 2018). Firstly, The Lisiecki and Raymo (2005) benthic isotope stack is used for comparison. By comparing peaks in the global benthic isotope record with the data generated in this study, the isotope versus depth profile may be tuned to an isotope versus age profile. Intervals that show a negative correlation between $\delta^{13}C$ and $\delta^{18}O$ are more indicative of patterns that globally influenced the isotope ratios. Therefore, for the non-mirroring intervals this approach is less reliable because the signal may not be of global origin.

3. Results

Not every single sample is included in the results, for several reasons. The first possible reason is that a data point is an outlier. The next reason for some samples being not taken into account is that the crags had very little material for picking. There is almost no sediment left after sieving for several samples (e.g. 214, 215 and 229 m). Also, sample 251 is missing due to there being not enough material left at the TNO depot, meaning that the sample was not taken to the lab. Samples 294, 297 and 299 m had unclear labeling and are therefore omitted as well. Other samples missing from the record is disregarded because they had too few forams.

3.1 Bulimina vs. Cassidulina

Several samples had enough of both *Bulimina and Cassidulina*. Both of these species were analyzed for these samples. The correlation between $\delta^{18}O$ of *Bulimina and Cassudilina* was worse than the correlation (R2 = 0.3734 Fig. 7) found in Noorbergen (2013).

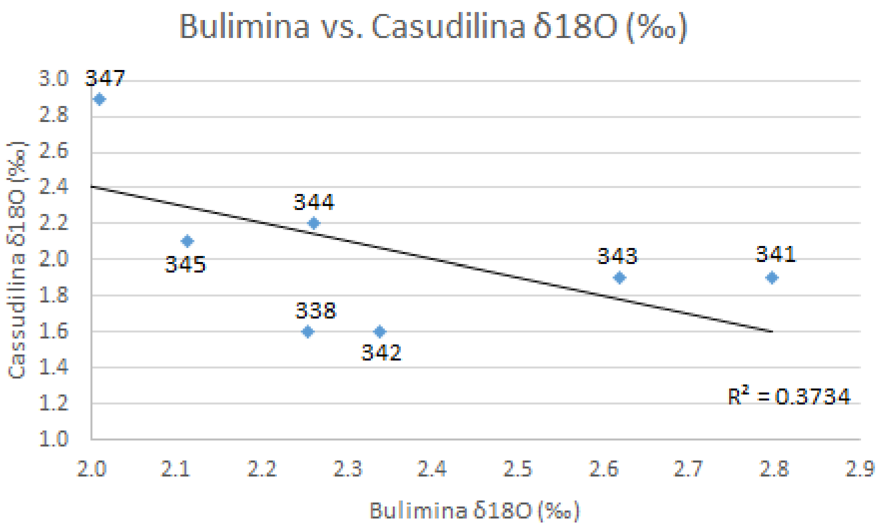

Figure 7. Correlation of δ18O between Cassidulina and Bulimina. Point labels indicate which depth the data originates from.

3.2 Stable isotopes

Results for stable oxygen isotope mass spectrometry generally are between 0 and 3‰, around an average of approximately 1.5‰ (Fig. 8). These values are plotted from high to low on the y-axis, as a higher $\delta^{18}O$ value indicates colder climate. There are several points that have negative $\delta^{18}O$.

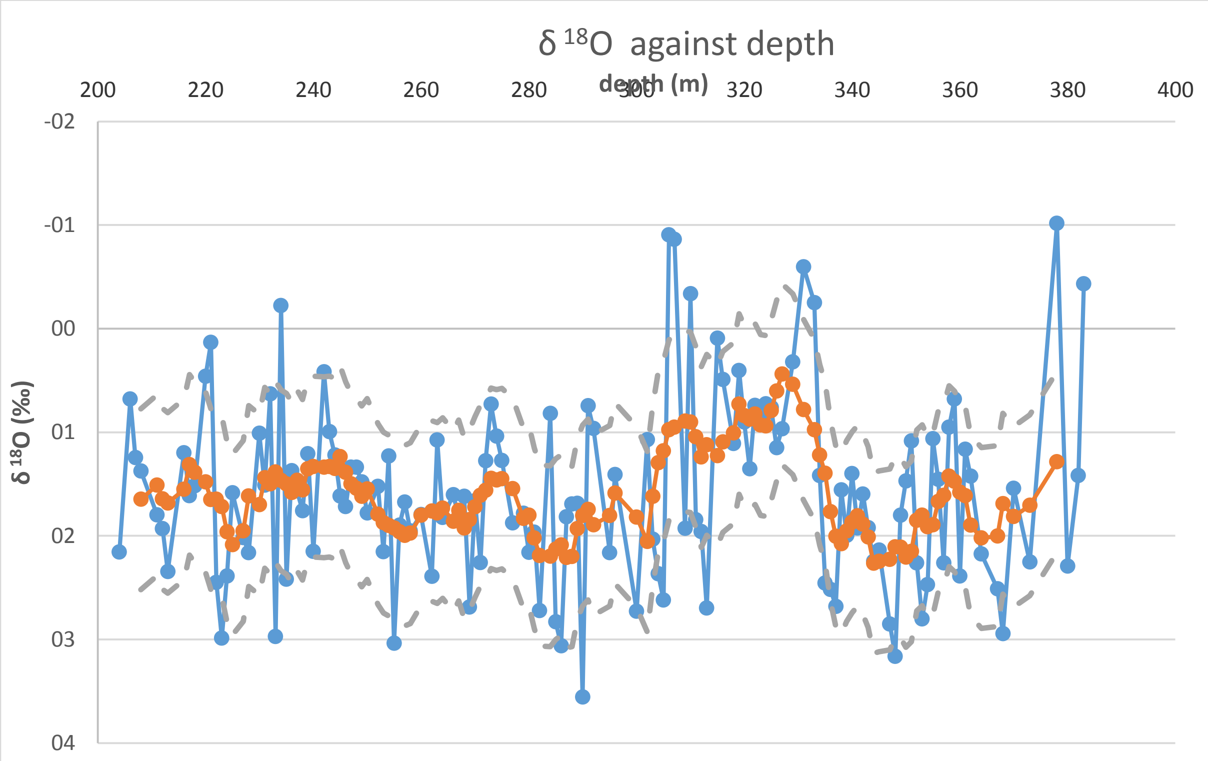

Figure 8. $\delta^{18}O$ against depth. Blue line indicates actual values measured by the gas bench. Orange line represents a 7-point moving average. Gray dashed lines represent added and substracted standard deviation from the 7-point moving average. Negative values for $\delta^{18}O$ are outliers, as well as every sample between 303 and 311 meters.

The data in Fig. 7 is plotted together with a 5-point moving average. Any point above the top gray line and below the bottom grey line (added and subtracted standard deviation, respectively) is regarded as an outlier and removed from the data (Fig. 8). These include the samples that had most extreme negative and positive values. There is one sequence, for the interval 303-311 m, where all samples are outliers. The other outliers seem to be more randomly distributed across the whole core.

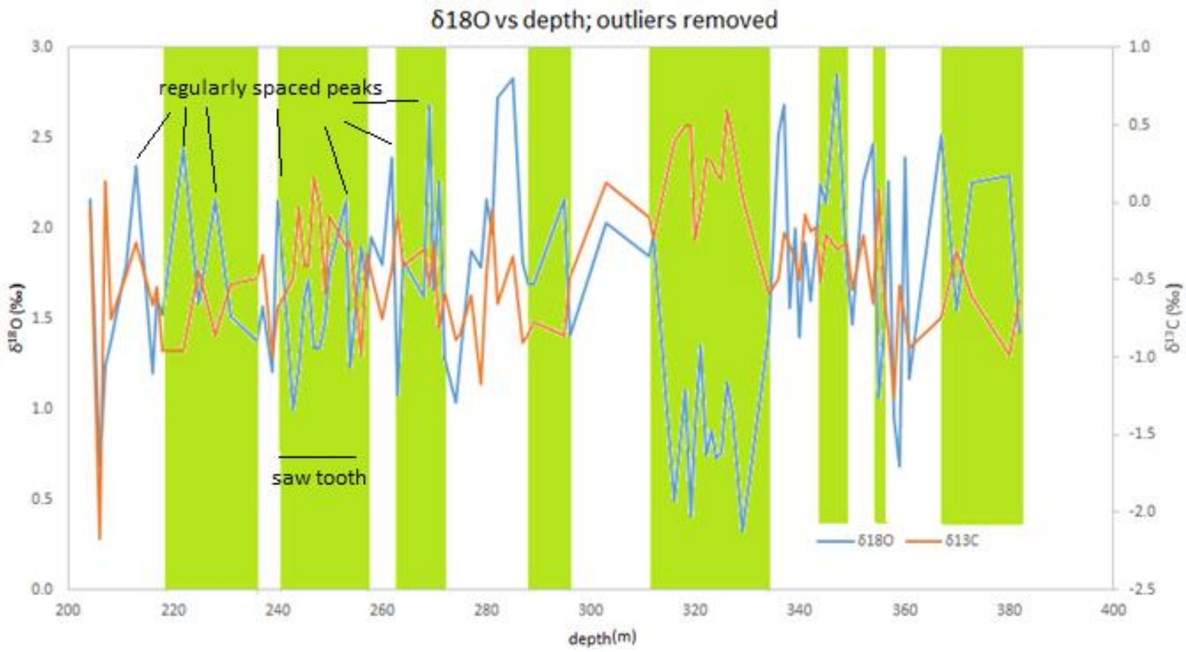

Figure 9. $\delta^{18}O$ (blue) plotted together with $\delta^{13}C$ (orange). Y-axis of $\delta^{18}O$ no longer inverted. Several parts(i.e. 316-329m) show a negative correlation, while for most of the record, a positive correlation between the two proxies can be seen.

After outlier-removal, the data shows values ranging from ~2.9 to ~0.3‰. Several striking patterns and features could be seen when looking at the remaining record. A “saw tooth pattern” could be seen, especially at the top 50 m of analyzed interval (Fig. 9). Within one saw tooth, $\delta^{18}O$ decreased slowly over time, while sudden rises followed the lowest values. Furthermore, there seemed to be no overall trend for the complete record. It showed no sign of either an increase or a decrease in $\delta^{18}O$. There was seemingly a cyclic pattern, with regular spaced peaks and valleys. However, any regularly spaced peaks in the depth domain do not necessarily indicate a regular cyclicity in the time domain.

The next striking feature was the sequence of low $\delta^{18}O$ values from 316 to 329 meters. This broader peak is preceded by a rapid drop in $\delta^{18}O$, and followed by a rapid increase. Also, the amplitude at these low values is smaller than those of the rest of the core.

The $\delta^{13}C$ record shows a variability of approximately 2.1‰, with most values between -1.4 and 0.7‰, around an average of approximately -0.5‰. When plotted together, the $\delta^{13}C$ record shows comparable patterns to the $\delta^{18}O$ record. However, this is not throughout the whole core. Some intervals show a negative correlation (green shaded intervals, Fig. 8). This was the most clear for the interval from 311 to 329 m, where $\delta^{13}C$ shows a strong increase where $\delta^{18}O$ shows the lowest values. However, the smaller peaks within this broad peak seem to have positive correlation. The intervals 225-230m, 279-287m and 355-382 also show this pattern, along with other, smaller intervals. For the rest of the record, $\delta^{13}C$ and $\delta^{18}O$ show a more positive correlation. Overall, $\delta^{13}C$ variability contains a smaller amplitude (~0.7‰ for most cycles) than that of the $\delta^{18}O$ (~1.0‰ for most cycles).

3.3 Lisiecki and raymo

The Lisiecki and Raymo stack for the same time interval as the Hank core shows similarities, mainly the saw tooth pattern describing the glacial interglacial cyclicity (Fig. 10). Apart from this, there are a number of major differences. The first difference being a linear rising trend (~0.3‰/Ma) over the LR04 Stack, towards the Pleistocene. $\delta^{18}O$ values for this study showed a slightly decreasing trend. The next major difference is the absolute $\delta^{18}O$ values. Where the LR04 stack varies between 2.7 to 3.9‰, results for this study generally varied between 0.3 and 2.8‰. Ergo, the variance is bigger (1‰ and 0.3-0.7‰, respectively), but the absolute values are smaller.

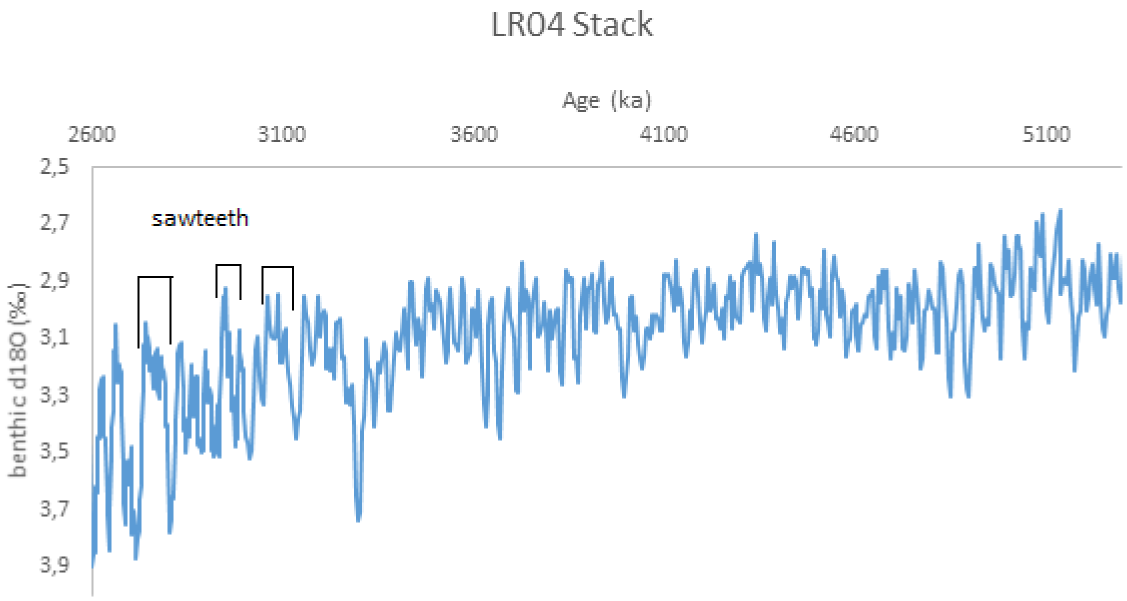

Figure 10. LR04 stack between 2600-5100, several extreme highs can be seen. A saw tooth pattern characterizes the youngest few cycles (Lisiecki and Raymo, 2005).

3.4 Northern Atlantic Ocean

Hank's sediment succession originates from the Northern Atlantic Ocean. Therefore it may make more sense to not take the global stack, but one individual record from the Northern Atlantic. One record has been provided by Risebrobakken et al. (2016), who took their core from off the coast of Norway, in the Nordic Seas. One peculiar detail about their results is that their absolute isotope values resemble Lisiecky and Raymo's data more than the data in this study. This is probably due to the location of Risebrobakken et al. (2016) being more open marine.

3.5 Other Proxies

Looking at the other data that was made available, it becomes clear that none of the proxies reflect each other at first glance (Fig. 11). Only the interval 311-329m shows some similarities for only some of the records with $\delta^{18}O$. The gamma values showed a sudden shift towards low values. MAT showed no real relation with $\delta^{18}O$. SST reconstructions based on alkenones did show similar patterns as $\delta^{18}O$, but again, only on the interval 311-329m.

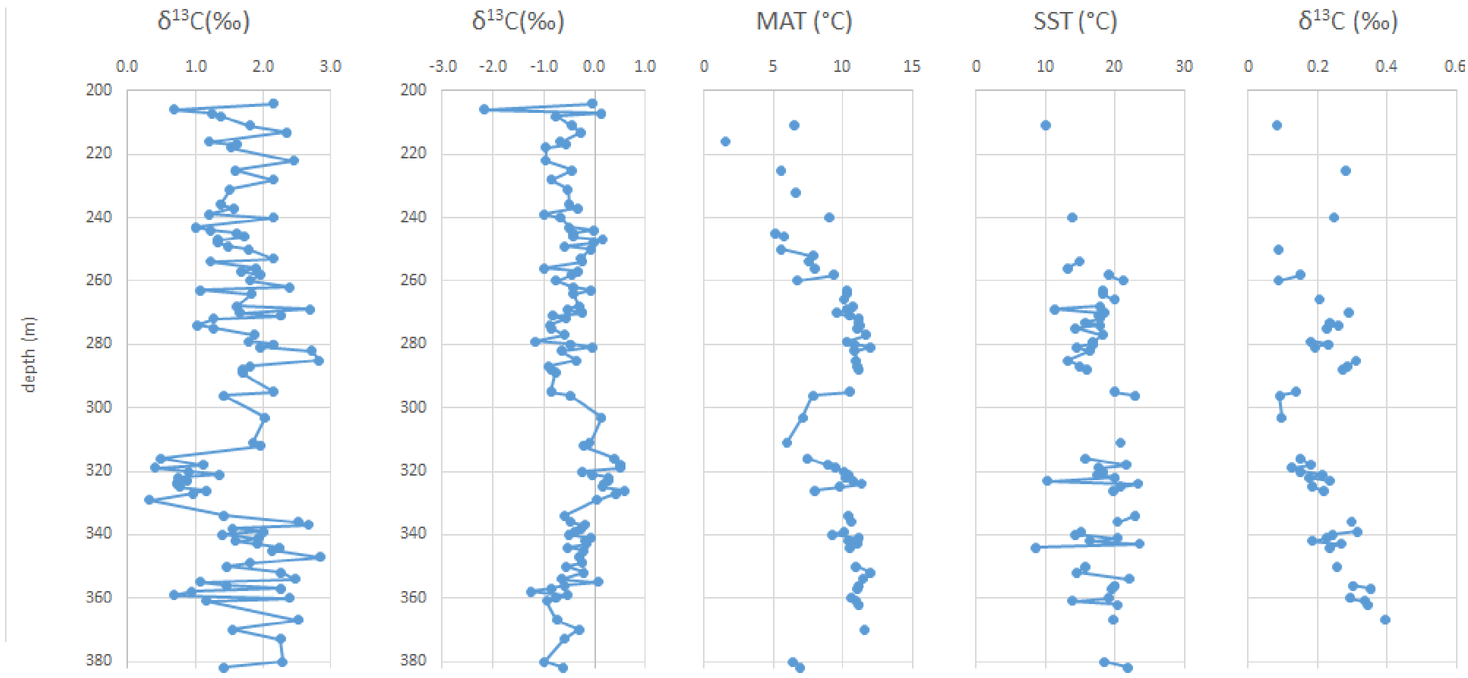

Figure 11. Available proxies plotted against depth. SST based on alkenones.

The dinoflagellate against sporomorph data (Fig. 12) shows a distinct shift from marine depositional environment to terrestrial, between 287 and 187 meters. This trend is non-existent at first, with few exceptions. There is a sharp peak at 306 m, and at 384 m there is a broader peak. After the peak at 306 meters, the environment becomes gradually more terrestrial. Superimposed on this trend is an apparent cyclicity. From 189 m upwards, the environment is predominantly terrestrial. This trend can also be seen in the seismic data and the lithologic section, where coarsening upwards between 295-210 m indicates a shift from marine to terrestrial environments.

Somewhere around 330m, there is an unconformity, as indicated by the seismic section (Fig. 5). Comparison with the other records may facilitate pinpointing this unconformity exactly. Apparently, when looking at the gamma ray record, there is a sudden shift in trend at 332 m. It can be argued that this marks the unconformity. More of these patterns can be seen, but not necessarily in each of the SP, resisivity and gamma ray records. The SP and resistivity records also hint at an unconformity at 186 m, and also at 160 m. The SP record shows a distinct peak at 394 m. This is most likely an erosional unconformity, which is typical in the Middle-Late Pliocene (Thöle et al., 2014). This unconformity formed during times of prograding delta.

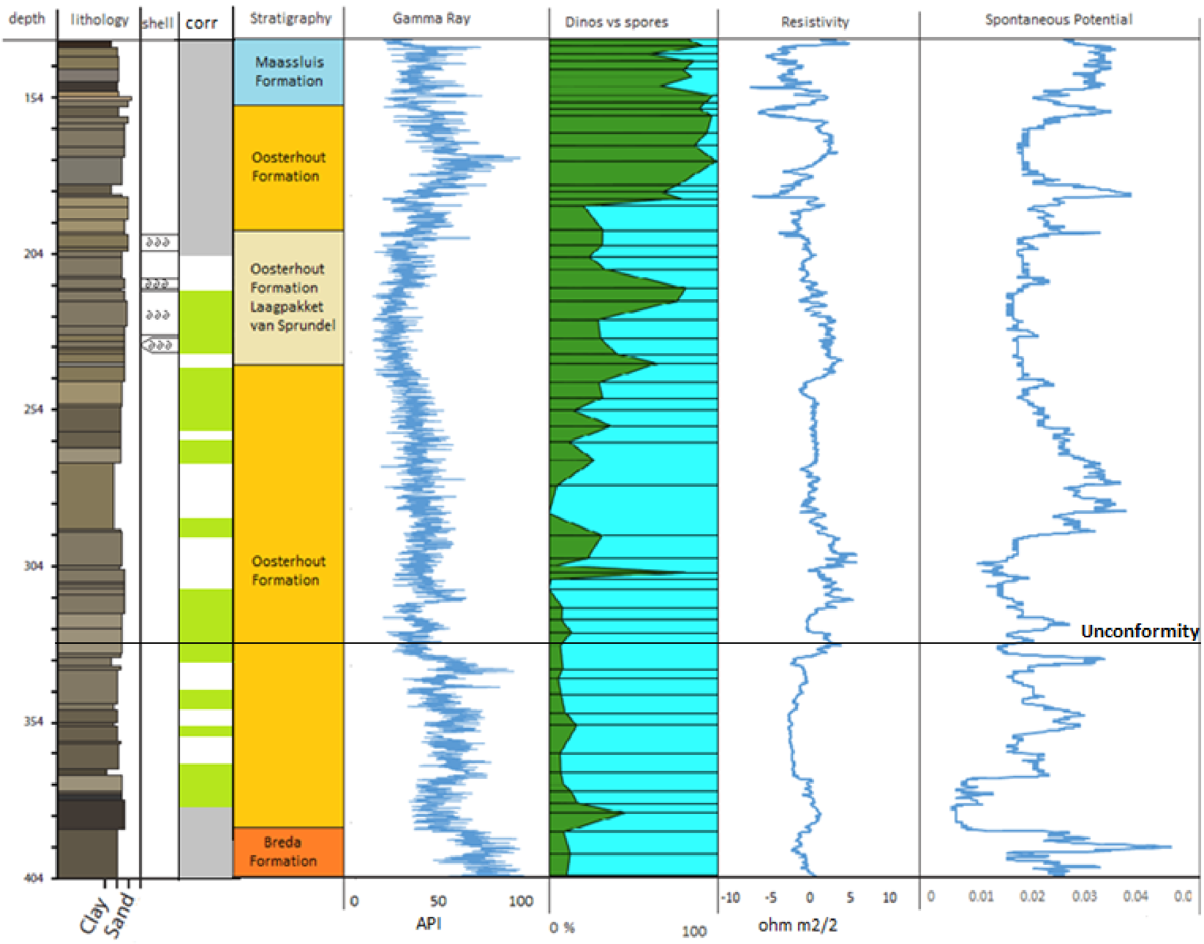

Figure 12. Lithological description using Munsell color chart. Crag layers indicated by symbols in second column. Green parts in third column shows what intervals have negative correlation between C and O isotopic ratios (see results). Gray parts have no data. Green and blue column shows dinoflagellate (blue) versus sporomorph (green) data (Munsterman, 2016). Intervals with a stronger relative abundance of dinoflagellates indicate a marine depositional environment. Resistivity in the second-to-right column is detrended.

3.6 Principal Component & Frequency analysis

The two principal components resulting from PCA have eigenvalues of 0.344 and 0.210, which means that, combined, they explain over half the variance in all records. The results PCA showed several distinct features (Fig. 13). The first being that the $\delta^{18}O$ record apparently shows great correlation with the GR log. This is something that could already be seen in figure 16. The GR log was the longest vector and was therefore most important. MAT lies closely to the x-axis, meaning that MAT is only influenced by one major factor, or may even describe that factor. The second factor (the y-axis) influenced the isotope records, both negatively. $\delta^{13}C$ seemed to be more closely related to SST, but is the shortest vector. SP is almost fully negatively correlated to $\delta^{13}C$.

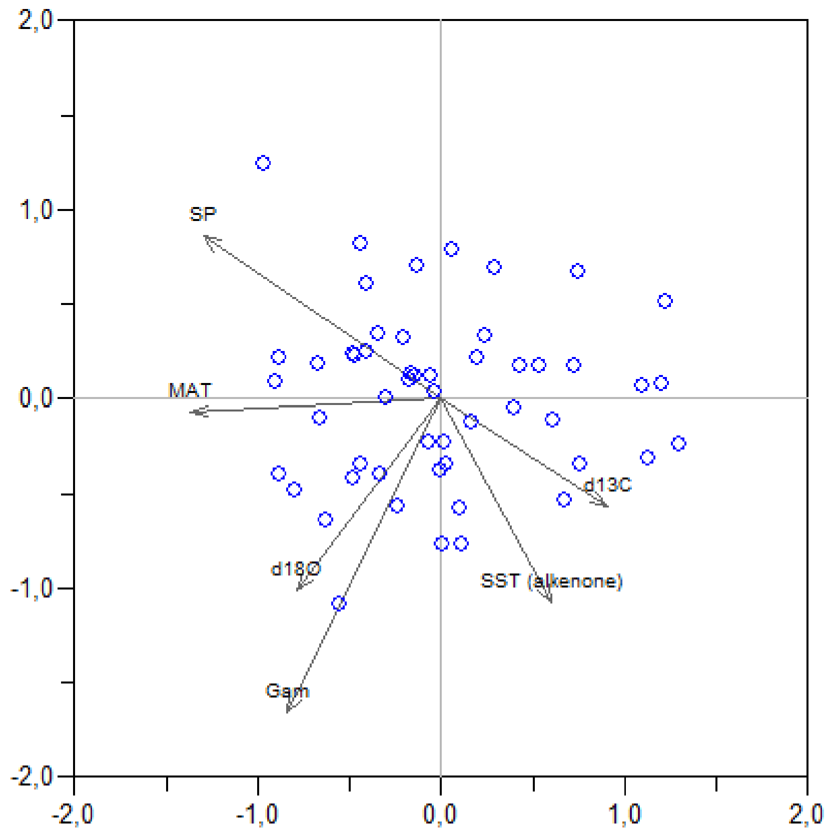

Figure 13. PCA of available proxies, except organic δ13C due to its limited sample size. Gamma ray (GAM) is most important and related to δ18O.

The data for $\delta^{18}O$ against age shows that the cyclicity which was visible before could still be seen (Fig. 14). Note that this is not tuned age, but simply the isotope ratio plotted against age, based on the extrapolated trend lines from Fig. 3. Results on frequency analysis were solely based on the upper part of the core (200-300 m) due to the resolution on the lower part being too low. Several distinct peaks could be distinguished. The saw tooth pattern described before becomes even more distinct.

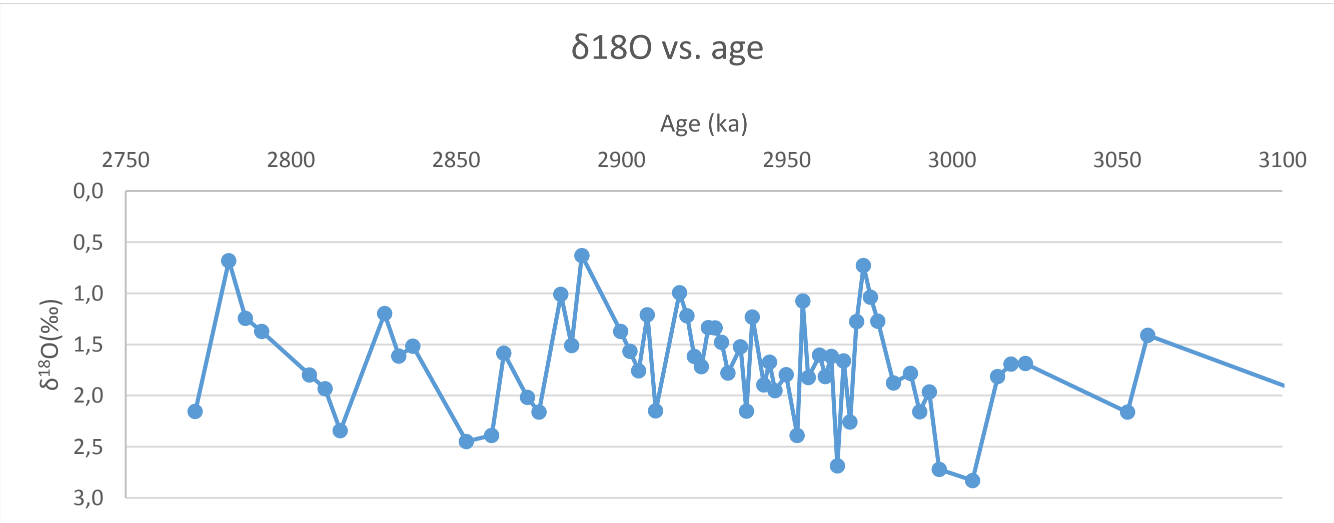

Figure 14. δ18O against age. Age based on age points made by Dearing Crampton Flood et al., 2018. Saw tooth pattern can be seen for the largest part of the record. After 3000ka, the resolution becomes distinctly lower, and data points are, therefore, not plotted in this figure.

There are several outstanding peaks of periods with the highest power (Fig. 15). These peaks were (in order of strongest to weakest): 46.3 kyr, 165.7kyr and 21.5 kyr. The other peaks were regarded as either artificial or as background noise. The periods of Milankovitch orbital climate variability are ~41 kyr, ~23kyr and ~100kyr. It becomes clear that the periods of the most dominant cycles in the power spectrum are slightly different to those of Milankovitch. This was most likely due to the high uncertainty range of the age points that were used to create the age model used for frequency analysis.

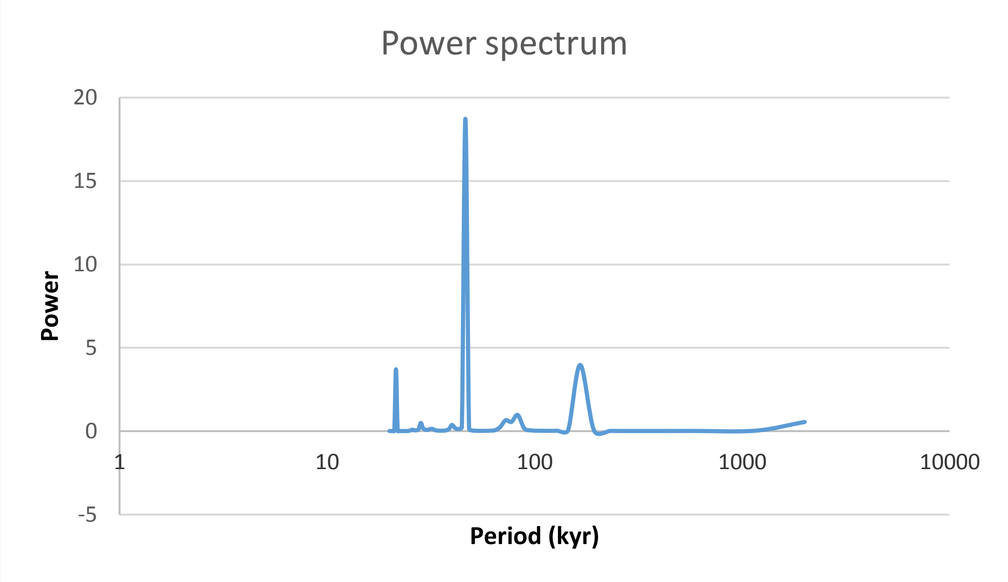

Figure 15. Power spectrum from interval 204-303 m.

Creating a Gaussian filter around the strongest peaks gave suboptimal results. Because the periods are slightly off, the cycles continuously come in and out of phase (Fig. 16). Also, the amplitude of precession cyclicity varies over time due to the effect of Eccentricity, which is superimposed on precession. This was not seen in the filtered precession on $\delta^{18}O$, at least not in a similar way. Therefore, creating an age model based on this analysis proves to be too challenging.

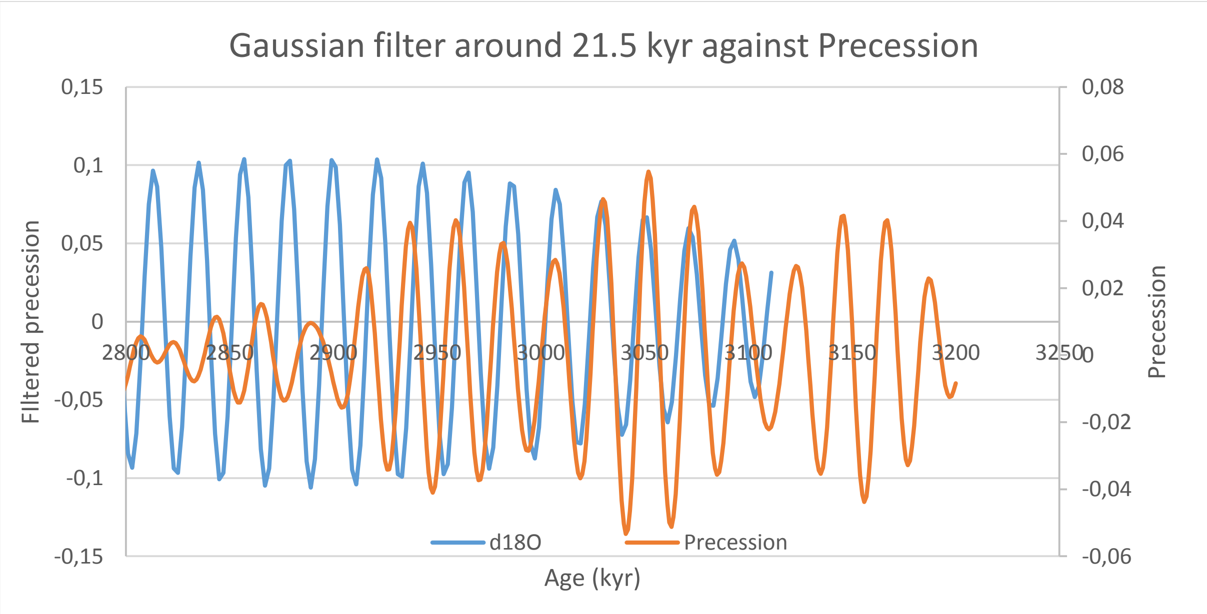

Figure 16. Gaussian filter for Precession (blue) for the interval 204-303 m, plotted with actual precession (orange) from 2800-3200 ka. Shifts in and out of phase due to slightly different periodicity.

4. Discussion

4.1 Age model

At some points in the record, a distinct saw tooth pattern is seen. Usually, this saw tooth pattern is the result of glacial-interglacial cyclicity. Periods of slow cooling are generally followed by rapid terminations (Broecker and Donk, 1970). Interestingly, the saw tooth pattern on the youngest few cycles are reversed in that regard. This could provide a clue as to which glacial or interglacial events they belong. The LR04 stack contains several of these “backwards” cycles as well, events G15, G17, and to a lesser extent G17 and G19 (Fig. 17). It is therefore concluded that these cycles may be correlated to our data.

Some caution is necessary when pinpointing these saw-tooth patterns to certain patterns in the LR04 stack. Not all saw teeth fall (entirely) in intervals with negatively correlated $\delta^{18}O$ and $\delta^{13}C$. This means that these patterns may be artificial, due to local sea level change, caused by phenomena such as an avulsion of the proto-Rhine or tectonic forcing.

Because of the low resolution at greater depth (>330m), no representative age model can be made for that part of the core. It cannot be said for certain that a high value in $\delta^{18}O$ correlates to a peak in the LR04 stack, and thus a glacial event. Also, because only some of the interglacials were useful for comparison with the LR04 stack, cycles had to be counted to ensure that no events were skipped between two interglacials, which could be pinpointed. Counting cycles on a Milankovitch scale is difficult if the resolution is so low that the time it takes to deposit one meter of sediment is longer than a singular cycle.

The creation of this age model is based on several arguments. When counting cycles after the unconformity, there is the right amount of cycles, starting from MG1, until G11 (Fig. 17). The shape and amplitude of cycles resemble each other as well. The youngest events also fall within the age uncertainty range of the previous age model based on last occurrences of dinoflagellates. However, the discrepancy between ages in this age model and the old age model becomes bigger when moving down in the succession. The isotope data and the $\delta^{13}C$ of organic matter, show distinct high amplitude variations at depth interval 303 - 311 meters. MAT shows relatively low temperatures around that interval. The sporomorph vs dinoflagellate data shows a dramatic increase in relative sporomorph abundance. Therefore, The M2 event is placed between 303 and 311 meters. This is still within the age uncertainty of the older age model. The observation that no *Cassidulina* were present anymore from 200 meters upwards should not mean that the Pleistocene-Pliocene boundary is defined there. The broad beak in the GR record could resemble the relatively stable and warm period starting from the end of G10. This also fits with MAT, which shows stable high values between 174 and 200 meters. However, the dinoflagellates against sporomorph record, as well as the seismic section shows a distinct shift from marine to terrestrial environment. Still, this could simply be the result of the prograding delta, supported by higher sediment rates.

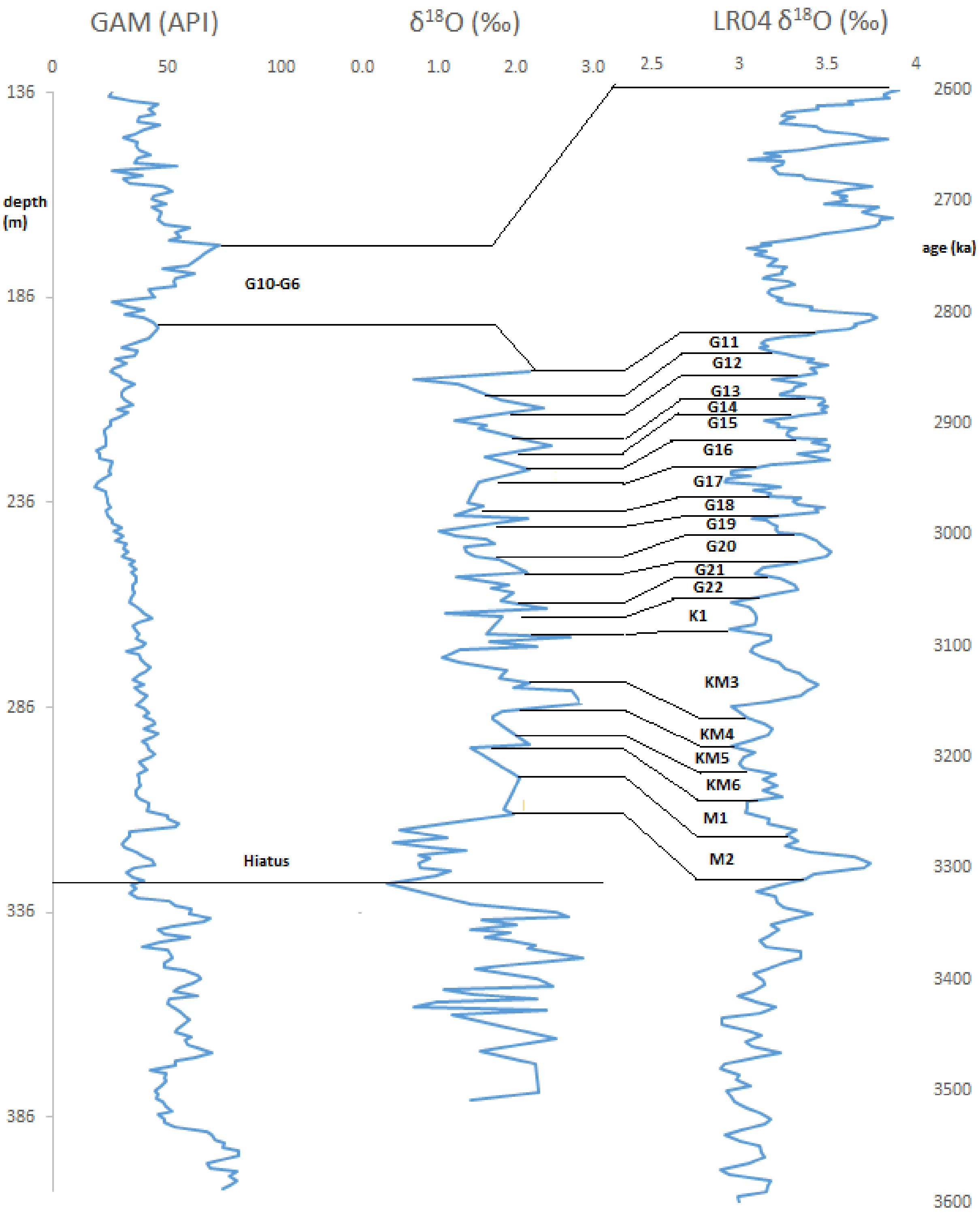

Figure 17. Age model, based on interglacial stages, seismic section and other previously mentioned proxies.

The borders of a glacial are loosely defined in Fig. 17. The important part is the peak of interglacials, which this age model is based on. By searching for the age of a peak in the LR04 stack, and assigning that age to a peak within this study's $\delta^{18}O$ record, the tuning presented in Fig. 18 can be plotted. Assuming constant sedimentation, a fairly accurate estimate of the age of sediments between the interval of 204 – 320 meters can be interpreted.

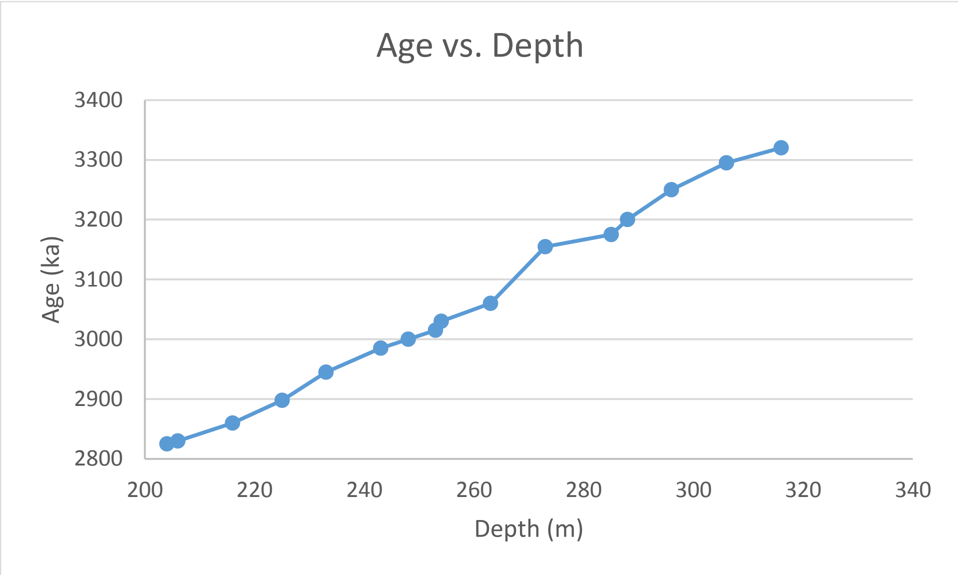

Figure 18. Tuning based on interglacial stadials. After comparison with the LR04 stack, several corrections were made.

The $\delta^{18}O$ record can then be plotted against age for this interval. When plotted against the LR04 stack, some minor corrections can be made, or extra age points can be added. The resulting record then resembles the LR04 stack relatively well, albeit that the low resolution intervals (e.g. 303 - 311 meters) does not show any peaks or valleys (Fig. 19).

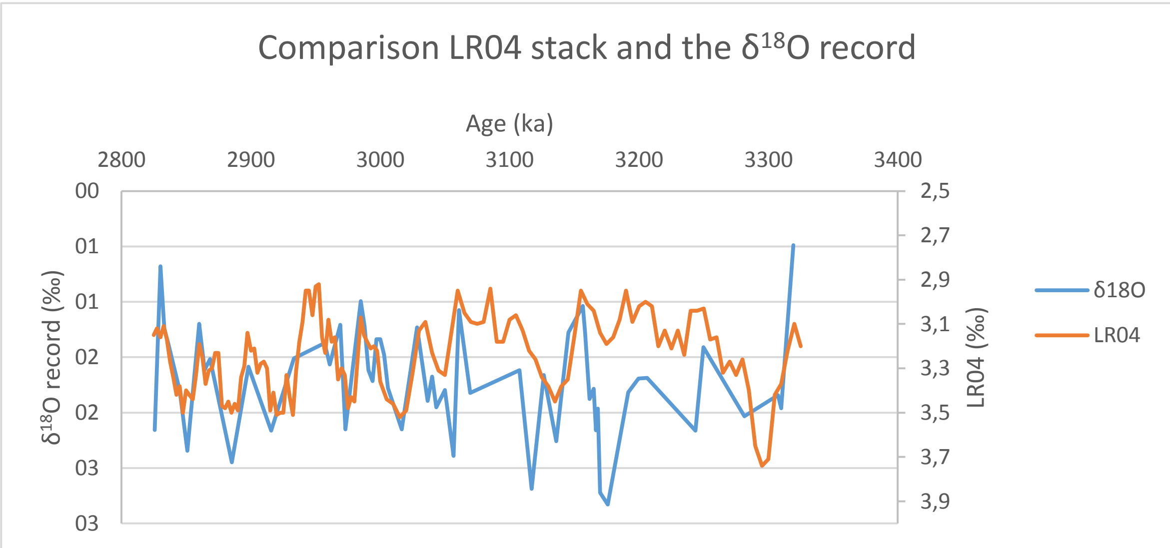

Figure 19. LR04 stack against this study's $\delta^{18}O$ record

4.2 Laboratorial uncertainties

Some intervals contained few forams. This results in having little material to use for mass-spectrometry. Ideally, a sample would weigh between 20-30 µg. Several samples (especially around 300 m) barely weighed 10 µg. Also, every complete run of approximately 60 samples had a different standard deviation. But during the last run, after measuring and correcting, this standard deviation should not exceed 0.05. However, it was 0.22 and 0.1 for carbon and oxygen isotopes, respectively.

The low abundance of *cassidulina* in some intervals also led to a greater variety of usable forams. Thus, slight differences in size and life cycle of picked forams was unavoidable. This was avoided for most samples, but not all. This problem was most prevalent at interval 300-312 and anywhere below ~370 meters. Also, forams were not crushed (see discussion in section 2.1). As such, some material within the chambers of individual forams may interfere with the measurement, however, results on both crushed and non-crushed samples showed that there was only a small difference (~0.3‰) between the two methods.

Lastly, results may vary due to water in the gas chamber of the instrument. This is seemingly unavoidable, because of the molecule's polarity, making it stick to the side of the chamber and making it impossible to remove (Van Dijk, personal communication). The gas bench can correct for this automatically, after data has been gathered. The uncertainty of data produced by the gas bench rises when air or water from the outside reaches the sample. Such a leak can happen when the lid on the vial is not closed properly, or there is some residue of acid or rubber resting on the vial, a consequence of improperly cleaned vials. A leak is represented in the results as an unnaturally high peak in nitrogen dioxide (NO_2) concentration. 15 samples had small leaks, but were still usable, because the small leak could be corrected for.

4.3 Geologic uncertainties

There are several uncertainties which are the result of the choice of location. Firstly, the location of the Hank borehole lies close the Proto-Rhine river delta. (Westerhoff, 2009) As a consequence, there are several factors contributing to noise or other disturbance of the isotope record. Firstly, an enhanced fresh water input can alter the $\delta^{18}O$ composition of surrounding waters. This is because $\delta^{18}O$ does not only reflect water temperature, but also salinity. This problem could be remedied by picking species that burrow deeper in the sediment, but that solution is not ideal. The sediment housing these species is easily disturbed, due to wave working, for example. This not only damages the test of the foram, but can also displace them. For this reason, creating an age model is not straightforward for intervals where the highest fresh water input is expected. These intervals are most likely the glacials. During colder periods, sea level drops and rivers can prograde. It can be argued that the Hank core lies even more proximal to the coast during times when the proto-Rhine delta builds its way into the North Sea.

As previously mentioned, for some intervals there is a negative correlation between $\delta^{18}O$ and $\delta^{13}C$, and for others there is no real correlation to be found. The major difference between these records and the Hank core is the location. The intervals in our record where $\delta^{13}C$ is highest (e.g. 311-336 m and 244-248 m) show negative correlation between $\delta^{13}C$ and $\delta^{18}O$, while these are expected to be the marine intervals. This can be explained by a higher vegetation density during interglacials. More vegetation means that more sediment (and thus organic material) gets trapped. As a result $\delta^{13}C$ does not decrease as much as expected.

The absolute values of $\delta^{18}O$ are much smaller than those of the LR04 stack. Other studies around the Nordic Seas (thus likely to have similar temperatures) show similar absolute $\delta^{18}O$ values to those of the LR04 stack (Risebrobakken et al., 2016). Therefore, the low $\delta^{18}O$ values from the Hank core must be explained by changes in salinity. The Hank core lies proximal to the coast and to a river delta. Fresh water input by the proto-Rhine decreases salinity and also $\delta^{18}O$ in turn (Delaygue et al., 2001). Salinity changes may also explain the difference in amplitude of the $\delta^{18}O$ swings. This is slightly counterintuitive as lower temperatures (thus higher $\delta^{18}O$) should lead to lower salinity (thus lower $\delta^{18}O$), and work in ways of negative feedback. However, during interglacials, enhanced runoff due to an increase in Alpine glacier melt water may increase the amplitude. Only comparing peaks and valleys between our data and the LR04 stack may not be sufficient, as individual peaks are difficult to assign an age to. This is because of the high uncertainty range of the age points in the current age model.

Nevertheless, the sporomorphs vs dinoflagellate data shows that these intervals reflect a mainly marine environment around those intervals. The only exception is the spike in dinoflagellate abundance at 384 m. The intervals with almost no correlation mainly above 244 meters, with few exceptions. Around that interval, moving forward in time, there is a gradual but certain increase in relative sporomorph abundance, indicating a more terrestrial environment. Superimposed on this is an apparent cyclicity going from more terrestrial towards more marine, and vice versa.

There is a distinct peak in sporomorph abundance at 306 m. Furthermore, every sample between 303 and 311 m was considered an outlier in the stable isotope data, and the biggest shifts in stable isotope composition occurred in this interval.

In short, the intervals which have a negative correlation between both isotope records are more useful in terms of tuning. These intervals generally reflect interglacial stages. Isotope data anywhere else in the record is too influenced by fresh water input. During glacials, eustatic sea level drops in the Northern Atlantic made way for progradation of the proto-Rhine river. Inversely, when sea level rises during interglacial stages, the environment becomes more marine and starts to reflect ice sheet volume and water temperature more, which is further indicated by the seismic data (Fig. 20).

4.4 Unconformities

There is a high uncertainty concerning changes in sedimentation rate between 265 and 330 m. The main focus lies with the potential unconformity at around 320 m, since it is the only one within the range of the stable isotope record. The hiatus is reflected in the $\delta^{18}O$ record which shows a sudden and rapid increase at this point.

There are multiple possibilities for the position and age of the unconformity between 3.3 and 4.5 Ma. An unconformity at this depth can be expected when looking at the previous age model, which predicts the M2 event (~3.3 Ma, a major glacial event, Lisiecki and Raymo, 2005) to be around 330 m. Before the M2 event, during late sea level high stand, progradation took place. When sea level started to fall due to lower temperatures, progradation continued, but due to lowering of the delta front, erosion of previously deposited topsets took place, creating an erosional surface. During late low stand (at the end of M2), the delta front aggrades, locally depositing new (coarse) sediment. This is further indicated when looking at the lithological description. Bottom- and foresets deposited during low stand are later eroded when sea level rises and the delta front retrogrades. After this, when sea level becomes more stable, the delta progradates, something which is characterized by coarsening upwards and laterally deposited parasequences.

Another possibility is that it is a non-depositional unconformity. The depositional environment was open marine, and sedimentation rates were low, as indicated by the previous age model. At any point

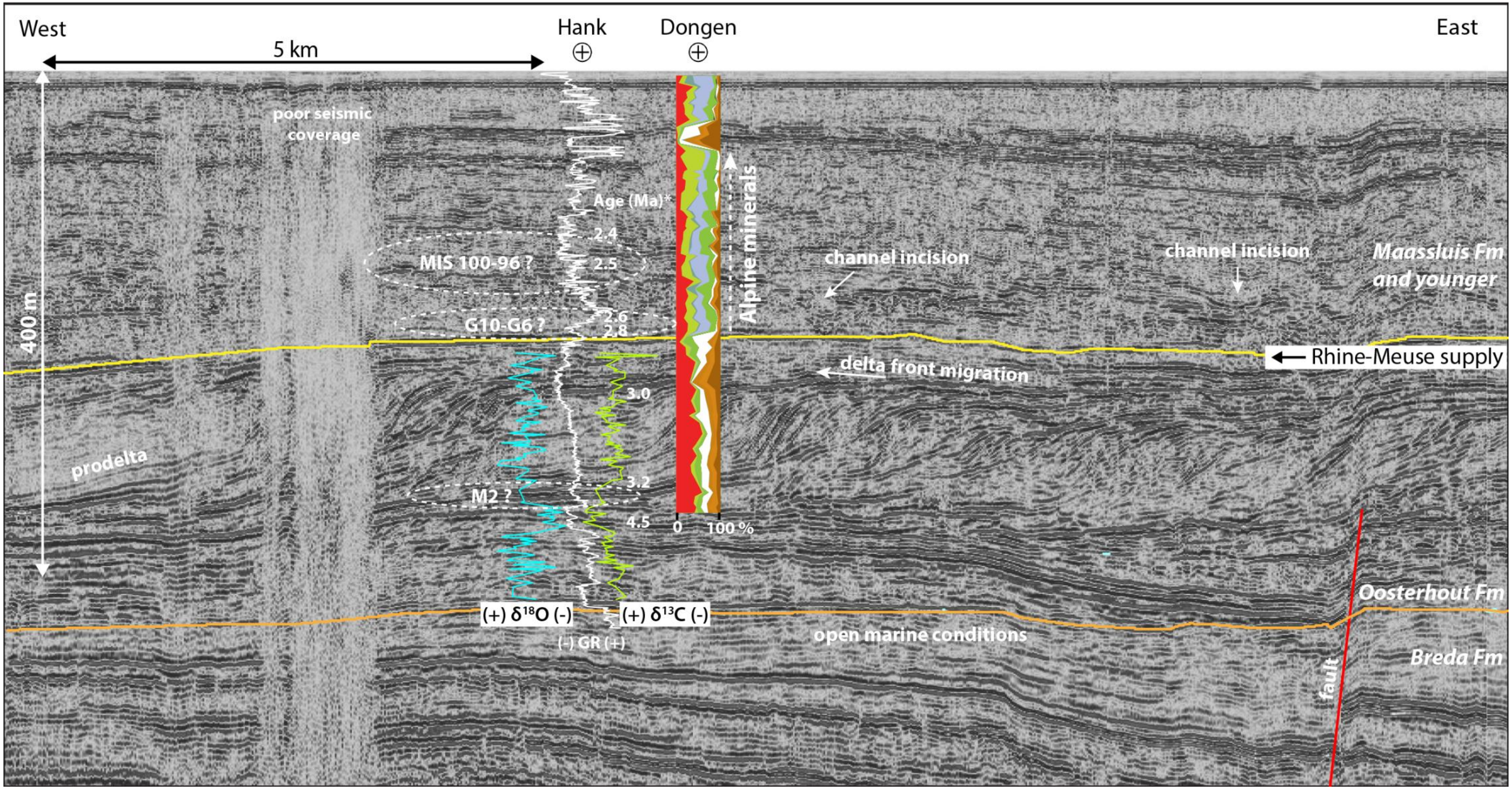

Figure 20. Seismic section around hank core, showing smoothed gamma ray (white), $\delta^{18}O$ (blue) and $\delta^{13}C$ (green). Mineral data from Westerhoff, 2009. Red, green and gray colors are indicative of Alpine minerals. Yellow line indicates the start of the Rhine Meuse supply, with Alpine minerals (Dirk Munsterman, personal communication).

in time, there may have been very little sediment entering the basin. The sandy lithology at this depth may then be explained by winnowing, a process which segregates finer material. This is then most likely during an interglacial, when sea level was highest. A relatively warm period before the M2 event seems a good candidate. This provides a challenge regarding the creation of an age model, as this raises the question whether the M2 event is recorded in the isotope data or not. One argument in favor of this is the distinct peak in sporomorph abundance at 306 meters. Many other proxies, such as the isotope data and MAT, show distinct high amplitude variations at this depth. However, they are not necessarily a result of colder temperatures. For instance, the sea surface temperature proxy does not show a tendency towards colder temperatures at this depth. After outlier removal, there is a positive excursion for the interval 311-303m, indicating climate cooling. The fact that every individual sample in this interval is an outlier may be caused by freshwater input effects.

Going upwards in the core, outside the range of the isotope data, there were several other indications of unconformities. There are peaks and/or valleys in resistivity and SP at 194, 186, 159 and 154 m. Sudden changes in lithology at these depths are also indicative of these unconformities.

A sudden shift in mineral composition of the sediment possibly showed contact between the Rhine river and the Alps (Fig. 20). Generally, the minerals originating from the Alps are more easily erodible than others (Westerhoff, 2009). The heavy minerals garnet (red), epidote (light green) and hornblende (green) are typically of Alpine origin (Hagedorn and Boenigk, 2008). The data shows that the alpine influence during the upper part of the core is relatively big. The distinct peak in non-Alpine minerals indicates that the Rhine river did not flow into the basin, but rather other Belgian rivers, with different origin.

Other unconformities at higher in the succession may either be caused by lack of sedimentation (e.g. avulsions) or by erosion. Because of the depositional environment (topset), erosional unconformities would likely only form during forced regression. A sudden increase in sediment, coupled with sea level drop would cause erosion inland. More runoff and erosion during glacials because of lack of vegetation would contribute to higher sediment input. However, there is no evidence pointing towards this.

4.5 Frequency analysis

The three major peaks in the power spectrum (Fig. 15) reflect roughly the periods of Milankovitch orbital cycles, albeit slightly different. Unfortunately, no reliable age model can be made using filtered obliquity or precession, as discussed previously. However, the relative dominance of Obliquity over Precession for the interval between 204 and 303 meters indicates something about forcing mechanisms. Obliquity shifts the polar circle over a range of latitudes. Consequently, obliquity influences climate on the highest latitudes more than on the lower latitudes. Then, as obliquity is more dominant, it is expected that meltwater coming from polar ice sheets mostly influences the $\delta^{18}O$ record. Precession has the opposite effect. If precession were dominant, meltwater from Alpine glaciers coming in as runoff through the proto-Rhine would be more influential on the $\delta^{18}O$ record.

5. Conclusion

The choice of location for this study (proximal to the coast) has made establishing and interpreting an age model more difficult. Many local processes (seismics, variations in runoff and deposition rates) can disturb the isotopic composition of a foraminifer's test. This leads to some challenges. Absolute isotopic values, as well as the amplitude of variation, differ from those of the LR04 stack. Frequency analysis bears no satisfactory result, as conversion from depth to time domain is not accurate enough to give cyclicity which is comparable to Milankovitch scale climate variability.

The next challenge is that only part of the $\delta^{18}O$ record is useful in comparing to the LR04 stack, as too many intervals are influenced by local disturbances. Only intervals which show a negative correlation between $\delta^{18}O$ and $\delta^{13}C$ are useful for comparison. These intervals are deposited during interglacials. Because sea level was higher, sediment layers formed in a more marine depositional environment, which is less prone to disturbance.

Other data sets greatly facilitate creating an age model, such as the sporomorph against dinoflagellate data and the seismic section. The final age model had to be created with depositional environment and delta morphology in mind. This in combination with glacial-interglacial cyclicity gives a clearer image of North Sea climate during the Pliocene (give approx. ranges of the age model that works best for the 'good' intervals). The age model provided in this study coincides with the previously published age model based on last occurrences of dinoflagellates relatively well. Glacial cycles are clearly visible and countable. But because of abovementioned uncertainties, one potential pitfall is that cycles have been appointed to certain depths by visual inspection only.

There is some room for improvement regarding the research on this particular area. A more complete age model could have been created when considering not only *Cassidulina* and *Bulimina* for mass spectrometry. Maybe other species that are most abundant from 200 meters upwards could be useful as well, provided that this new species reacts to temperature and fresh water input the same as *Cassidulina* and *Bulimina.* A simple solution to avoid this problem altogether is choosing a location that is more distal to the coast, where interference of freshwater input is much less. However, that would impede the comparison between terrestrial and marine proxies. Because the Pliocene North Atlantic climate is so important as an analogue to future climate projections, future research is necessary.

Acknowledgements

I would like to thank all my supervisors on giving me the opportunity to carry out this research, for providing me with the necessary tools and literature to get started, and for their feedback. Lars Noorbergen is especially thanked for all the help on several different aspects and disciplines needed to create this age model. I would also like to thank the people who have helped me in the lab, especially Arnold van Dijk. Timme Donders and Dirk Munsterman are thanked for their help with the understanding of the other proxies.

References

Boschman, C. (2016). Sea Surface Temperature proxy comparison for the Pliocene North Sea.

Broecker, W. S., & Donk, J. (1970). Insolation changes, ice volumes, and the O18 record in deep-sea cores. *Reviews of Geophysics*, *8*(1), 169-198.

Delaygue, G., Bard, E., Rollion, C., Jouzel, J., Stiévenard, M., Duplessy, J. C., & Ganssen, G. (2001). Oxygen isotope/salinity relationship in the northern Indian Ocean. *Journal of Geophysical Research: Oceans*, *106*(C3), 4565-4574.

De Schepper, S., Gibbard, P. L., Salzmann, U., & Ehlers, J. (2014). A global synthesis of the marine and terrestrial evidence for glaciation during the Pliocene Epoch. *Earth-Science Reviews*, *135*, 83-102.

De Schepper, S., Schreck, M., Beck, K. M., Matthiessen, J., Fahl, K., & Mangerud, G. (2015). Early Pliocene onset of modern Nordic Seas circulation related to ocean gateway changes. Nature communications, 6.

Doppert, J.W.Chr. (1980): Lithostratigraphy and biostratigraphy of marine Neogene deposits in the Netherlands. Mededelingen Rijks Geololgische Dienst, 32: 16, 255-311

Dearing Crampton Flood, E., Peterse, F., Munsterman, D., & Sinninghe Damste, J. (2016, April). A terrestrial Pliocene-Pleistocene temperature record from North-Western Europe. In *EGU General Assembly Conference Abstracts* (Vol. 18, p. 7408).

Dowsett, H. J., Chandler, M. A., & Robinson, M. M. (2009). Surface temperatures of the Mid-Pliocene North Atlantic Ocean: implications for future climate. *Philosophical Transactions of the Royal Society of London A: Mathematical, Physical and Engineering Sciences*, *367*(1886), 69-84.

Dowsett, H. J. (2007). The PRISM palaeoclimate reconstruction and Pliocene sea-surface temperature. *Deep-time perspectives on climate change: marrying the signal from computer models and biological proxies*, 459-480.

Ebbing, J.H.J. & De Lang, F.D. (2003). *Formatie van Oosterhout.* Retrieved from https://www.dinoloket.nl

Fontanier, C., Jorissen, F. J., Licari, L., Alexandre, A., Anschutz, P., & Carbonel, P. (2002). Live benthic foraminiferal faunas from the Bay of Biscay: faunal density, composition, and microhabitats. *Deep Sea Research Part I: Oceanographic Research Papers*, *49*(4), 751-785.

Hagedorn, E. M., & Boenigk, W. (2008). The Pliocene and Quaternary sedimentary and fluvial history in the Upper Rhine Graben based on heavy mineral analyses. *Netherlands Journal of Geosciences-Geologie en Mijnbouw*, *87*(1), 21.

Herfort, L., Schouten, S., Boon, J. P., & Damsté, J. S. S. (2006). Application of the TEX86 temperature proxy to the southern North Sea. *Organic Geochemistry*, *37*(12), 1715-1726.

Juggins, S. (2007). C2: Software for Ecological and Palaeoecological Data Analysis and Visualisation (User Guide Version 1.5). *Newcastle upon Tyne: Newcastle University*, 77.

Kuhlmann, G., Langereis, C. G., Munsterman, D., Leeuwen, R. J. V., Verreussel, R., Meulenkamp, J. E., & Wong, T. E. (2006). Integrated chronostratigraphy of the Pliocene-Pleistocene interval and its relation to the regional stratigraphical stages in the southern North Sea region. *Netherlands Journal of Geosciences/Geologie en Mijnbouw*, 85(1), 19-35.

Lisiecki, L. E., & Raymo, M. E. (2005). A Pliocene-Pleistocene stack of 57 globally distributed benthic δ18O records. *Paleoceanography*, *20*(1).

Lisiecki, L. E., & Raymo, M. E. (2007). Plio–Pleistocene climate evolution: trends and transitions in glacial cycle dynamics. *Quaternary Science Reviews*, *26*(1-2), 56-69.

Londeix, L., Benzakour, M., Suc, J. P., & Turon, J. L. (2007). Messinian palaeoenvironments and hydrology in Sicily (Italy): the dinoflagellate cyst record. Geobios, 40(3), 233-250.

Louwye, S., Head, M. J., & De Schepper, S. (2004). Dinoflagellate cyst stratigraphy and palaeoecology of the Pliocene in northern Belgium, southern North Sea Basin. Geological Magazine, 141(03), 353-378.

Mackensen A., Schumacher S., Radke J. Schmidt D.N., 2000. Microhabitat preferences and stable carbon isotopes of endobenthic foraminifera: clue to quantitative reconstruction of oceanic new production? *Marine Micropaleontology* 40, 233 – 258.

McCorkle, D. C., Keigwin, L. D., Corliss, B. H., & Emerson, S. R. (1990). The influence of microhabitats on the carbon isotopic composition of deep-sea benthic foraminifera. *Paleoceanography*, *5*(2), 161-185.

Meijer, T., Cleveringa, P., Munsterman, D. K., & Verreussel, R. M. C. H. (2006). The Early Pleistocene Praetiglian and Ludhamian pollen stages in the North Sea Basin and their relationship to the marine isotope record. Journal of Quaternary Science, 21(3), 307-310.

Mensink, H. & Menkovic, A. (2003) Description of Hank sediment core. *TNO, Geological Survey of The Netherlands.*

Mudelsee, M., & Raymo, M. E. (2005). Slow dynamics of the Northern Hemisphere glaciation. *Paleoceanography*, *20*(4).

Mudie, P. J. (1987). Palynology and dinoflagellate biostratigraphy of deep-sea drilling project Leg-94, Site-607 and Site-611, North Atlantic Ocean. Initial Reports of the Deep Sea Drilling Project, 94, 785.

Munsterman, D. K., & Brinkhuis, H. (2004). A southern North Sea Miocene dinoflagellate cyst zonation. *Netherlands Journal of Geosciences*, *83*(4), 267-285.

Munsterman, D.K. (2016). Towards a higher resolution: The Plio-Pleistocene palynostratigraphy of well B44E0146 (Hank), interval 45-404 m. *TNO, Geological Survey of The Netherlands, 1-13.*

Noorbergen, L.J. (2013). Early Pleistocene benthic stable isotopes in the netherlands: A first approach.

Noorbergen, L. J., Lourens, L. J., Munsterman, D. K., & Verreussel, R. M. C. H. (2015). Stable isotope stratigraphy of the early Quaternary of borehole Noordwijk, southern North Sea. *Quaternary International*, *386*, 148-157.

Overeem, I., Weltje, G. J., Bishop-Kay, C., & Kroonenberg, S. B. (2001). The Late Cenozoic Eridanos delta system in the Southern North Sea Basin: a climate signal in sediment supply?. *Basin Research*, *13*(3), 293-312.

Paillard, D., Labeyrie, L. D., & Yiou, P. (1996). AnalySeries 1.0: a Macintosh software for the analysis of geophysical time-series. *Eos*, *77*, 379.

Ravelo, A. C., & Andreasen, D. H. (2000). Enhanced circulation during a warm period. *Geophysical Research Letters*, *27*(7), 1001-1004.

Raymo, M. E., Grant, B., Horowitz, M., & Rau, G. H. (1996). Mid-Pliocene warmth: stronger greenhouse and stronger conveyor. *Marine Micropaleontology*, *27*(1-4), 313-326.

Raymo, M. E., Lisiecki, L. E., & Nisancioglu, K. H. (2006). Plio-Pleistocene ice volume, Antarctic climate, and the global δ18O record. *Science*, *313*(5786), 492-495.

Raymo, M. E., Mitrovica, J. X., O'Leary, M. J., DeConto, R. M., & Hearty, P. J. (2011). Departures from eustasy in Pliocene sea-level records. *Nature Geoscience*, *4*(5), 328-332.

Rider, M.H. (1986). The Geological Interpretation of Well Logs. Blackie and Son Limited & Halsted Press, 1, 27-175.

Risebrobakken, B., Andersson, C., De Schepper, S., & McClymont, E. L. (2016). Low-frequency Pliocene climate variability in the eastern Nordic Seas. *Paleoceanography*, *31*(9), 1154-1175.

Robinson, M. M., Dowsett, H. J., & Chandler, M. A. (2008). Pliocene role in assessing future climate impacts. *Eos, Transactions American Geophysical Union*, *89*(49), 501-502.

Ruddiman W.F. (2014) Earth's climate past and future, New York: *W.H. Freeman and company* (445p.).

Shackleton, N. J., Backman, J., Zimmerman, H. T., Kent, D. V., Hall, M. A., Roberts, D. G., ... & Huddlestun, P. (1984). Oxygen isotope calibration of the onset of ice-rafting and history of glaciation in the North Atlantic region. *Nature*, *307*(5952), 620.

Thöle, H., Gaedicke, C., Kuhlmann, G., & Reinhardt, L. (2014). Late Cenozoic sedimentary evolution of the German North Sea–A seismic stratigraphic approach. *Newsletters on Stratigraphy*, *47*(3), 299-329.

Van Balen, R. T., Houtgast, R. F., Van der Wateren, F. M., Vandenberghe, J., & Bogaart, P. W. (2000). Sediment budget and tectonic evolution of the Meuse catchment in the Ardennes and the Roer Valley Rift System. *Global and Planetary Change*, *27*(1-4), 113-129.

Versteegh, G. J. M., Bosch, H. J., & De Leeuw, J. W. (1997). Potential palaeoenvironmental information of C 24 to C 36 mid-chain diols, keto-ols and mid-chain hydroxy fatty acids; a critical review. Organic Geochemistry, 27(1), 1-13.

Westerhoff, W.E., 2009. Stratigraphy and sedimentary evolution: the lower Rhine–Meuse system during the Late Pliocene and Early Pleistocene (southern North Sea Basin). *PhD thesis*, Vrije Universiteit Amsterdam.

Appendix

Depth	#cass.	#bul.	#plank.	Note	Depth	#cass.	#bul.	#plank.	Note
404	0	0	0		353	7	3	6	
403	0	0	0		352	6	2	3	
402	0	0	0		351	9	0	8	
401	0	0	0		350	12	2	9	
400	0	0	0		349	16	0	7	
399	0	0	0		348	23	1	7	
398	0	0	0		347	16	1	10	LO Uvigerina
397	0	0	0		346	33	1	11	
396	0	0	0		345	10	2	9	
395	0	0	0		344	26	2	15	
394	2	1	0		343	24	2	6	
393	0	0	0		342	14	2	7	
392	0	0	0		341	18	7	11	
391	0	1	0		340	15	8	25	
390	3	11	5		339	16	0	12	
389	2	2	2		338	32	2	17	
388	0	0	0		337	23	4	11	
387	0	0	0		336	12	0	6	
386	0	0	0		335	12	1	4	
385	0	0	0		334	9	5	4	
384	7	0	0		333	9	2	4	
383	8	0	0		332	10	0	1	
382	7	1	3		331	6	1	6	
381	0	0	0		330	7	1	3	
380	7	0	0		329	7	0	2	
379	0	1	0		328	10	1	6	
378	7	0	0		327	9	0	6	
377	0	0	0		326	7	0	9	
376	2	0	0	Taken from smaller faction	325	8	0	3	
375	0	0	0		324	12	0	2	
374	0	0	0		323	11	0	3	
373	8	0	5		322	8	0	2	
372	0	0	0		321	7	0	1	
371	0	0	0		320	7	1	1	
370	7	0	3		319	8	0	0	
369	0	0	0		318	7	1	2	
368	10	1	3		317	2	1	2	
367	7	0	0		316	5	3	3	
366	7	1	6		315	7	2	2	
365	11	2	11		314	9	0	0	
364	11	6	5		313	7	2	2	
363	8	4	9		312	8	0	0	
362	6	4	8		311	7	0	0	
361	20	3	8		310	6	0	0	
360	7	4	8		309	7	1	3	
359	6	6	4		308	3	1	0	
358	13	6	20		307	6	1	5	
357	8	0	7		306	4	1	1	
356	8	0	7		305	7	3	0	
355	8	5	12		304	8	3	2	
354	9	1	4		303	11	6	6	

Depth	#cass.	#bul.	#plank.	Note	Depth	#cass.	#bul.	#plank.	Note
302	13	3	2		251				Too little material left at TNO
301	8	0	5		250	7	0	1	
300	0	0	0		249	7	1	0	
299				Unsure labelling, non-picked	248	9	0	3	
298	7	2	8		247	7	0	8	
297				Unsure labelling, non-picked	246	8	0	4	
296	6	0	0		245	7	1	1	
295	7	0	0		244	7	0	1	
294				Unsure labelling, non-picked	243	6	0	3	
293	8	0	0		242	7	0	7	
292	7	1	3		241	0	0	0	
291	9	2	2		240	7	0	0	
290	9	1	1		239	8	0	7	
289	9	1	8		238	7	0	5	
288	8	1	0		237	8	0	0	
287	13	0	3		236	7	0	2	
286	11	0	2		235	8	0	1	
285	8	1	2		234	7	0	1	
284	7	0	1		233	7	0	0	
283	7	0	3		232	5	0	0	
282	9	0	1		231	7	0	0	
281	8	0	2		230	5	1	0	
280	9	0	4		229	5	1	1	
279	7	0	0		228	8	0	0	
278	13	0	2		227	7	0	1	
277	8	0	0		226	0	0	0	
276	8	2	0		225	7	0	1	
275	11	3	1		224	8	0	0	
274	7	0	3		223	7	1	0	
273	12	0	1		222	6	0	1	
272	5	1	0		221	8	0	0	
271	7	0	1		220	9	0	0	
270	10	0	1		219	4	2	0	
269	8	0	1		218	7	0	0	
268	5	2	3		217	7	0	1	
267	7	0	0		216	7	0	0	
266	8	0	1		215	0	0	0	Almost only shell material
265	7	0	2		214	0	0	0	Almost only shell material
264	7	0	0		213	11	0	1	
263	8	0	2		212	7	0	1	
262	8	0	2		211	5	4	0	
261	7	0	2		210	7	0	1	
260	10	0	5		209	6	0	0	
259	7	0	0		208	9	0	0	
258	11	1	3		207	7	1	3	
257	7	0	1		206	4	0	0	
256	8	0	1		205	5	0	0	
255	9	0	4		204	7	0	0	
254	7	0	1		203	0	0	0	
253	6	0	1		202	0	0	0	
252	8	0	9		201	0	0	0	